EXPANDED USE OF BICYCLIC GUANIDINATE LIGANDS IN DIMETAL PADDLEWHEEL COMPOUNDS

A Dissertation

by

MARK DAVID YOUNG

Submitted to the Office of Graduate Studies of
Texas A&M University
in partial fulfillment of the requirements for the degree of

DOCTOR OF PHILOSOPHY

May 2009

Major Subject: Chemistry

EXPANDED USE OF BICYCLIC GUANIDINATE LIGANDS IN DIMETAL PADDLEWHEEL COMPOUNDS

A Dissertation

by

MARK DAVID YOUNG

Submitted to the Office of Graduate Studies of
Texas A&M University
in partial fulfillment of the requirements for the degree of

DOCTOR OF PHILOSOPHY

Approved by:

Co-Chairs of Committee,	Carlos A. Murillo
	Marcetta Y. Darensbourg
Committee Members,	Paul A. Lindahl
	George Kattawar
Head of Department,	David Russell

May 2009

Major Subject: Chemistry

ABSTRACT

Expanded Use of Bicyclic Guanidinate Ligands in Dimetal Paddlewheel Compounds.

(May 2009)

Mark David Young, B.A., McDaniel College

Chair of Advisory Committee: Dr. Carlos A. Murillo

This dissertation concerns the use of bicyclic guanidinate ligands to prepare new dimetal paddlewheel compounds. Specifically, Ru_2^{6+}, Re_2^{6+}, Re_2^{7+}, and Os_2^{7+} compounds will be examined to observe any changes brought about by using bicyclic guanidinate ligands with varying ring sizes. In the Ru_2^{6+} compounds, different ligand ring sizes cause a change in the electronic configuration and magnetic properties. Bicyclic guanidinate ligands allow the preparation of Re_2^{7+} compounds from Re_2^{6+} compounds, both of which are examined structurally and electrochemically. $[Os_2(hpp)_4]^+$ is examined to improve upon earlier studies, yielding a model of the *g*-tensor components with respect to the compound structure.

An additional project included in the dissertation involves the study of an asymmetric trinickel extended metal atom chain. The structural effects of the asymmetry are examined to help elucidate the magnetic behavior that differs significantly from symmetric trinickel extended metal atom chains.

DEDICATION

To the memory of Dr. F. Albert Cotton, that continues to inspire new efforts of discovery.

"If it isn't published, it isn't finished."

-Dr. Cotton

ACKNOWLEDGEMENTS

I would like to thank Dr. Cotton for the wonderful opportunity to work under his watchful eye on these projects. Even though events did not go as hoped, I cannot imagine a better place to have continued my studies.

I thank Dr. Murillo for the time and sacrifice he has provided to see me through. His expertise was an invaluable resource.

I thank Dr. M. Darensbourg for her contributions as Co-chair of my committee. I would also thank Dr. Lindahl and Dr. Kattawar for their service on my committee.

I would like to thank to thank the members of the Laboratory for Molecular Structure and Bonding that have helped me over the years. Specifically, I thank Dr. Chad Wilkinson for helping me start the guanidinate project, Dr. Qinliang Zhao for her help with Density Functional Theory calculations, and Dr. Gina Chiarella for her assistance with the work on rhenium. I would also like to thank Mrs. Julie Zercher for her hard work in helping to organize this and other group manuscripts.

I thank Dr. Naresh Dalal and Mr. Zhenxing Wang of Florida State University for their collaboration on the osmium project.

I thank Dr. Joe Reibenspies for help with X-ray structure determinations and Dr. Andrey Prosvirin for his assistance on magnetic susceptibility measurements.

Finally, I thank my friends and family who have supported me through the highs and lows of my graduate career.

NOMENCLATURE

hpp	The anion of 1,3,4,6,7,8-hexahydro-*2H*-pyrimido[1,2-*a*]pyrimidine
tbn	The anion of 1,4,6-Triazabicyclo[3.4.0]non-4-ene
tbo	The anion of 1,4,6-Triazabicyclo[3.3.0]oct-4-ene
dpa	The anion of 2,2'-dipyridylamine
EMAC	Extended Metal Atom Chain

TABLE OF CONTENTS

CHAPTER Page

LIST OF FIGURES

LIST OF TABLES

CHAPTER I

INTRODUCTION

In 1964 a shift was made in inorganic chemistry with the synthetic preparation of salts containing the $Re_2Cl_8^{2-}$ ion, which contains an unsupported bond between two metal atoms.[1] This was followed by the seminal work to confirm the existence of the quadruple bond formed by overlapping metal based d orbitals.[2] In the following years the number of transition metal atoms used to form dimetal compounds quickly expanded, owing to the use of carboxylates as bridging ligands.[3] Future advances came with newer ligands, such as hydroxypyridines and formamidinates, as shown in Scheme 1.

Scheme 1. Overview of ligands in dimetal compounds.

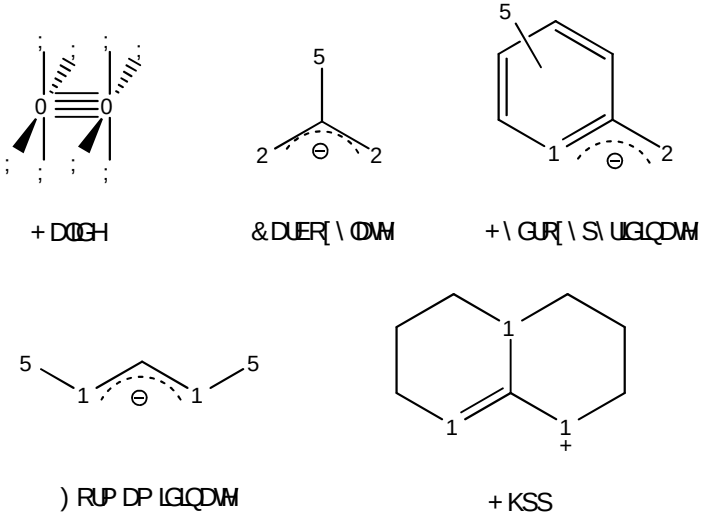

Formamidinates in particular have been very useful as supporting ligands in so-called “dimer of dimers” compounds,[4] which have been extremely productive in

---

This dissertation follows the journal style of *Inorganic Chemistry*.

increasing knowledge about possible linkers for molecular wires, an area of much ongoing research.[5] While other ligands have also been used in dimetal compounds, the most recent class that has attracted the most attention has been bicyclic guanidinates, beginning with Hhpp (1,3,4,6,7,8-hexahydro-*2H*-pyrimido[1,2-*a*]pyrimidine). While initially used for its expected stability in harsh conditions (under which formamidinates or triphenylguanidinate would be cleaved), it was quickly discovered to stabilize high oxidation states in dimetal compounds, such as the first niobium compound to contain a triple bond.[6] Additionally, hpp was found to interact strongly with the δ orbitals of dimetal species, raising them in energy and thus lowering the oxidation potential, leading to the discovery of a closed-shell molecule, $W_2(hpp)_4$, that had a lower onset ionization potential than elemental cesium.[7]

After the general properties of hpp as a ligand had been established, further work was performed in the hopes of expanding the capabilities of bicyclic guanidinates.[8] Specifically, there were two goals to be accomplished. The first was to increase the solubility of dimetal guanidinate complexes. This was accomplished by synthesizing two new guanidinate ligands with alkyl substituents, HTMhpp (3,3,9,9-tetramethyl-1,5,7-triazabicyclo[4.4.0]dec-4-ene) and HTEhpp (3,3,9,9-tetraethyl-1,5,7-triazabicyclo[4.4.0]dec-4-ene), shown in Scheme 2. The second goal was to expand the range of electrochemical potentials by adjusting the length of the metal-metal bond. To do this, new bicyclic guanidinate ligands were synthesized which had varying ring sizes. Combinations of ring sizes included 5,5 (1,4,6-Triazabicyclo[3.3.0]oct-4-ene, Htbo), 5,6 (1,4,6-Triazabicyclo[3.4.0]non-4-ene, Htbn), 7,5 (1,4,6-Triazabicyclo[3.5.0]dec-4-ene, Htbd) and 7,6 (1,5,6-Triazabicyclo[3.5.0]undec-5-ene, Htbu), also shown in Scheme 2.

This initial work was performed using molybdenum, and each ligand was used in a variety of oxidation states to provide a picture of how this dimetal system would respond.

Scheme 2. Bicyclic guanidinate ligands related to Hhpp.

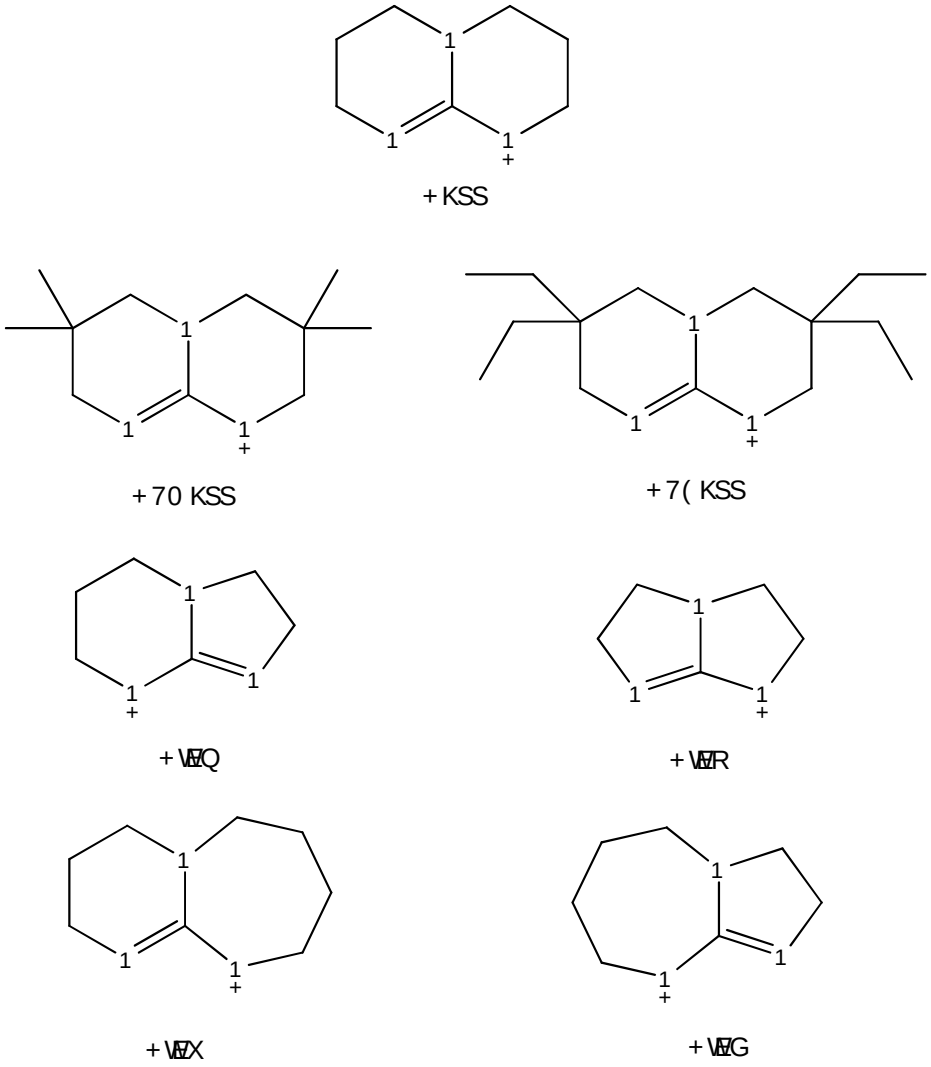

With this initial work now complete, additional work can now be done on other dimetal compounds to determine if the results seen for molybdenum apply to other metals, and if so, to what extent. In Chapter II diruthenium compounds prepared with the tbn and tbo ligands will be characterized. The focus of this study is on the magnetism of these two compounds and how it relates to the previously studied compound

$Ru_2(hpp)_4Cl_2$. Magnetic susceptibility studies, combined with variable temperature X-ray diffraction, will help to determine the electronic configuration of these compounds.

In Chapter III, the bicyclic guanidinate ligand in question will be hpp, paired with osmium as the metal. This work is a follow up to an earlier study in which the preliminary results showed a very unusual EPR spectrum. A powder sample gave a peak in the EPR spectrum with a very low *g* value of ~0.72 and an extremely large line width of approximately 6000 Gauss. New studies involving frozen solution samples and single crystal experiments are performed to obtain additional information from these spectra, including the identification of $g_{\parallel}$ and $g_{\perp}$.

Chapter IV relates a new study on dirhenium guanidinate compounds. The guanidinate ligands used are hpp, tbn, and tbo. Several compounds are examined in both the 6+ and 7+ oxidation states structurally and electrochemically. Additionally, the effects of axial ligands on the electrochemical potentials are examined.

Chapter V is not concerned with dimetal guanidinate compounds; rather, a trinickel chain is studied supported by the ligand dpa (the anion of 2,2'-dipyridylamine). Previous studies examined symmetric extended metal atom chains and the antiferromagnetic behavior demonstrated by these compounds that have no metal-to-metal bonds. Oxidized compounds were also prepared, with a surprising reduction in the metal-to-metal distances for what is described as a 3c-1e$^-$ bond. In the new work presented here, the axial ligands on either side of the trinickel chain are asymmetric. The effects of this asymmetry on the structure and magnetism on the Ni_3^{6+} chain are examined, and these results are then used to re-examine the previous conclusions of an oxidized Ni_3^{7+} metal chain.

Finally, Chapter VI summarizes the results from the various guanidinate projects to reach some overarching conclusions about the effects of these modified bicyclic guanidinate ligands. Possible future aims of this research and that of the extended metal atom chains are also presented.

CHAPTER II

SIGNIFICANT EFFECT OF LIGAND BITE ANGLE ON THE MAGNETISM OF DIRUTHENIUM GUANIDINATE COMPOUNDS

Introduction

Since 1964 when the first species containing a direct and unsupported quadruple bond between metal atoms, $Re_2Cl_8^{2-}$, was reported focus has been placed on the determination of the electronic configuration as a means of explaining various properties and behaviors in compounds with metal-to-metal bonds.[1] The "traditional" energy ordering of the orbitals of $\sigma<\pi<\delta<\delta^*<\pi^*<\sigma^*$ has been surprisingly useful especially for compounds containing eight or less bonding electrons but when electrons occupy antibonding orbitals it only serves as a starting point since in some cases the energy of the antibonding orbitals may be very similar and thus the above ordering may be an over-simplification.[3] Early examples are those of compounds containing Ru_2^{n+} cores (n = 4, 5, or 6), in which the δ^* and π^* orbitals are often nearly degenerate,[9] leading to variety in electronic structures depending on the identity of the bridging and axial ligands. Even though separating the effect of each effect is not always straightforward, fairly well-understood are the Ru_2^{6+} compounds for which the effect an axial ligand has been well described.[10,11,12] In these compounds which have 10 metal-based electrons, strong σ donors, such as cyanide and alkynyl ligands interact with the σ bonding orbitals of the ruthenium atoms, destabilizing them to such an extent that the ground state configuration becomes $\pi^4\delta^2\pi^{*4}$. Because the s bond is eliminated, a significant lengthening of 0.2–0.3

Å in the Ru–Ru bond is observed as weak s donor ligands such as Cl are replaced by alkynyl ligands in compounds of the type $Ru_2(amidinate)_4Cl_2$.[2] Less well understood has been the effect that the bridging ligands exert on the metal-based orbitals. With few exceptions, the majority of Ru_2^{6+} compounds contain bridged by *N*,*N*'-donor ligands, including aminopyridinates, formamidinates, and benzamidinates.[2]

As of yet there have been only two Ru_2^{6+} species with guanidinate bridging ligands, $Ru_2(hpp)_4Cl_2$[13] and $Ru_2(hpp)_4(CF_3SO_3)_2$[14] (hpp = the anion of 1,3,4,6,7,8-hexahydro-*2H*-pyrimido[1,2-*a*]pyrimidine). These compounds show an interesting magnetic behavior being paramagnetic with an $S = 1$ at ambient temperature but diamagnetic at very low temperature. A question that arose was whether this was due to a change in electronic configuration as the temperature changed. The high temperature behavior with two unpaired electrons was inconsistent with a $\sigma^2\pi^4\delta^2\delta*^2$ configuration and thus favored the $\sigma^2\pi^4\delta^2\pi*^2$ configuration indicating that the $\pi*$ orbital was lower in energy relative to the $\delta*$ orbital. The question that the magnetic measurements could not resolve unambiguously was whether the low temperature diamagnetism was due to a change in electronic configuration or some alternative effect. The answer to this question arose from careful structural measurements done at variable temperature.[14] The premise was that if the was a change in electronic configuration, transfer of two electrons from a p* orbital to a d* orbital would be accompanied by a measurable decrease in the metal-to-metal distance, a hypothesis that has since been shown to be true for some compounds with Ru_2^{5+} cores.[15] For $Ru_2(hpp)_4Cl_2$ and $Ru_2(hpp)_4(CF_3SO_3)_2$, crystallographic measurements at variable temperature showed that the Ru–Ru distances remained unchanged from 27 to 296 K which suggested that the change in magnetism was

unrelated to an change in electronic configuration and therefore due to a large zero-field splitting which contributed to the electron pairing in an A_{1g} (M_s = 0) state derived from a $^3A_{2g}$ configuration.[14,16]

In the present study the effect of the bite angle of the ligands on the Ru–Ru bond and magnetism of Ru_2^{6+} species with $Ru_2(guanidinate)_4^{2+}$ cores and their magnetism has been examined using a guanidinate ligand with two fused 5-membered rings (tbo = the anion of 1,4,6-triazabicyclo[3.3.0]oct-4-ene) and another one with a 5,6-membered ring (tbn = the anion of 1,4,6-triazabicyclo[3.4.0]non-4-ene). These and other analogous ligands have been useful for the preparation of quadruply bonded compounds with very interesting electrochemical, electronic and solubility properties.[17,18,19]

Experimental

All syntheses were carried out under inert atmosphere using standard Schlenk techniques unless otherwise noted. The ligand precursors Htbn, and Htbo were prepared according to the literature[17a] as was $Ru_2(OAc)_4Cl$.[20] Solvents were dried using a Glass Contour solvent system. Mass spectrometry data (electrospray ionization) were recorded at the Laboratory for Biological Mass Spectrometry at Texas A&M University using an MDS Series Qstar Pulsar with a spray voltage of 5 kV. Elemental analyses were performed by Robertson Microlit Laboratories, Inc., Madison, NJ. Infrared spectra were recorded in a Perkin-Elmer 16PC FT IR spectrophotometer using KBr pellets. Electronic spectra were recorded on a Shimadzu UV-2501 PC spectrophotometer. Variable-temperature magnetic susceptibility measurements were obtained from 2 to 300 K using a Quantum Design SQUID magnetometer MPMS-XL operated at 1000 G. These data were corrected for diamagnetism.

Synthesis of $Ru_2(tbn)_4Cl_2$, 1. To a mixture of solid $Ru_2(OAc)_4Cl$ (100 mg, 0.211 mmol) and Zn powder (100 mg, 1.53 mmol) was added 25 mL of THF. The resulting brick red suspension was stirred and gently refluxed overnight. The following morning the mixture was filtered using a fritted-glass packed with Celite giving a yellow filtrate. To this solution was added 1.0 mmol of Li(tbn), prepared by adding equimolar amounts of Htbn and BuLi in 25 mL of THF. The color immediately darkened and the mixture was stirred for thirty minutes. Afterwards, the solvent was removed under vacuum and 25 mL CH_2Cl_2 were added to the residue, producing a violet solution. After stirring for thirty minutes, the reaction mixture was exposed to air overnight. Crystals were obtained by layering hexanes onto a CH_2Cl_2 solution of **1**. Yield: 78 mg (48%). Mass spectrum, ESI^+: Calcd for $M–Cl^+$: 735 amu. Found: 735 amu. Anal. Calcd[21] for $C_{24}H_{40}N_8Cl_2Ru_2$: C, 37.45; H, 5.24%. Found: C, 37.38; H, 5.32%. IR: 2850 (m), 1628 (m), 1542 (s), 1444 (w), 1264 (m). UV-vis: λ_{max} 535 nm.

Synthesis of $Ru_2(tbo)_4Cl_2$, 2. To a mixture of solid $Ru_2(OAc)_4Cl$ (100 mg, 0.211 mmol) and Zn powder (100 mg, 1.53 mmol) were added 25 mL of THF. The resulting suspension was stirred and gently refluxed overnight. The following morning the yellow solution was filtered through Celite. To this was added 1.0 mmol of Li(tbo), prepared by adding an equimolar amount of BuLi to Htbo in 25 mL of THF. The solution immediately darkened and was stirred for 30 min. Afterwards, the solvent was removed via vacuum and 25 mL CH_2Cl_2 were added, producing a black solution. After stirring for 30 min, a septum in the flask was removed to expose the solution to air overnight. Crystals of **2** were obtained the following morning by allowing the solution to stand overnight without stirring. Yield: 86 mg (57%). Mass spectrum, ESI^+: Calcd for $M–Cl^+$:

679 amu. Found: 679 amu. Anal. Calcd for $C_{20}H_{32}N_8Cl_2Ru_2$: C, 33.66; H, 4.52%. Found: C, 33.26; H, 4.25%. IR: 2926 (m), 2852 (m), 1638 (m), 1509 (m), 1440 (w), 1263 (m), 1106 (m).

X-ray Structure Determinations. Data were collected on a Bruker SMART 1000 CCD area detector system. Cell parameters were determined using the SMART software suite.[22] Data reduction and integration were performed with the software SAINT.[23] Absorption corrections were applied by using the program SADABS.[24] The positions of the Ru atoms were found via direct methods using the program SHELXTL.[25] Subsequent cycles of least-squares refinement followed by difference Fourier syntheses revealed the positions of the remaining non-hydrogen atoms. Hydrogen atoms were added in idealized positions. All hydrogen atoms were included in the calculation of the structure factors. All non-hydrogen atoms were refined with anisotropic displacement parameters. In **1**, the tbn ligands were solved as an average over two orientations, as the asymmetric nature of the ligand rings was disordered. In **2**, the non-coordinating nitrogen atom was refined over two positions. Data collection and refinement parameters for **1** and **2** are summarized in Table 1. Selected bond distances and angles are listed in Tables 2 and 3 for **1** and **2**, respectively.

Results and Discussion

Syntheses. Even though the target compounds have Ru_2^{6+} cores, the syntheses were carried out by first reducing $Ru_2(OCCH_3)_4Cl$ with zinc powder in THF. The need of this somewhat convoluted procedure was necessary because ligand substitution on the easily accessible Ru_2^{5+} species was kinetically slow to be useful.[26] However, as indicated

Table 1. Crystallographic data for **1** and **2** at various temperatures.

Compound	**1**	**1**	**2**	**2**	**2**
Chemical formula	$Ru_2C_{24}H_{40}Cl_2N_{12}$	$Ru_2C_{24}H_{40}Cl_2N_{12}$	$Ru_2C_{20}H_{32}Cl_2N_{12}$	$Ru_2C_{20}H_{32}Cl_2N_{12}$	$Ru_2C_{20}H_{32}Cl_2N_{12}$
fw	769.72	769.72	713.62	713.62	713.62
Space group	*I*4/*m*	*I*4/*m*	*I*4/*m*	*I*4/*m*	*I*4/*m*
a (Å)	9.6352(8)	9.596(3)	8.911(1)	8.842(2)	8.827(2)
b (Å)	9.6352(8)	9.596(3)	8.911(1)	8.842(2)	8.827(2)
c (Å)	15.423(3)	15.425(9)	15.309(4)	15.289(4)	15.280(6)
V (Å^3)	1431.8(3)	1420.5(10)	1215.6(4)	1195.3(5)	1190.6(6)
Z	2	2	2	2	2
d_{calcd} (g·cm^{-3})	1.785	1.800	1.950	1.983	1.991
μ (mm^{-1})	1.281	1.291	1.501	1.526	1.532
T (K)	**213**	**30**	**213**	**70**	**30**
R1[a] (wR2[b])	0.0540 (0.0991)	0.0586 (0.1345)	0.0707 (0.1266)	0.0466 (0.0929)	0.0467 (0.0883)

[a] $R1 = [? w(F_o - F_c)^2 / ? wF_o^2]^{1/2}$.

[b] $wR2 = [? [w(F_o^2 - F_c^2)^2] / ? w(F_o^2)^2]^{1/2}$, $w = 1/[\sigma^2(F_o^2) + (aP)^2 + bP]$, where $P = [\max(F_o^2,0) + 2(F_c^2)]/3$.

Table 2. Selected bond lengths (Å) and angles (º) for **1**.

	213 K	**30 K**
Ru(1)–Ru(1a)	2.387(1)	2.387(3)
Ru(1)–Cl(1)	2.558(3)	2.585(5)
Ru(1)–N(1)	2.042(7)	2.039(8)
N(1)–C(3)	1.30(2)	1.38(3)
N(2)–C(3)	1.34(3)	1.32(3)
N(3)–C(3)	1.37(1)	1.43(2)
Cl(1)–Ru(1)–Ru(1a)	180	180
Ru(1)–Ru(1a)–N(2)	88.2(8)	89.0(10)
Ru(1a)–Ru(1)–N(1)	89.4(8)	91.0(10)
N(1)–C(3)–N(2)	121.8(7)	124.7(11)

Table 3. Selected bond lengths (Å) and angles (º) for **2**.

	213 K	**70 K**	**30 K**
Ru(1)–Ru(1a)	2.501(2)	2.503(3)	2.502(3)
Ru(1)–Cl(1)	2.490(3)	2.488(4)	2.487(5)
Ru(1)–N(1)	2.024(6)	2.033(7)	2.024(7)
N(1)–C(3)	1.304(7)	1.288(7)	1.305(8)
N(1a)–C(3)	1.304(7)	1.288(7)	1.305(8)
N(2)–C(3)	1.34(1)	1.34(2)	1.32(2)
Cl(1)–Ru(1)–Ru(1a)	180	180	180
N(1)–Ru(1)–Cl(1)	91.9(1)	92.1(2)	91.9(2)
Ru(1a)–Ru(1)–N(1)	88.2(1)	87.9(2)	88.2(2)
N(1)–C(3)–N(1a)	130.6(10)	131.8(11)	130.6(11)

by an immediate change in color of the reaction mixture, ligand substitution was fast upon addition of Li(tbn) or Li(tbo) to $Ru_2(OCCH_3)_4$, prepared in situ.

Structure Comparisons. At first glance, the molecular structures of **1** and **2**, shown in Figure 1, are analogous to that of $Ru_2(hpp)_4Cl_2$ having a paddlewheel structure with four equatorially bound guanidinate ligands and two axially coordinated chlorine atoms. However, inspection of the bond distances which are provided in Tables 2 and 3 for **1** and **2**, respectively, show a very large difference in Ru–Ru distances with that for **1** (2.387(1) Å at 213 K) being 0.11 Å shorter than that in **2** (2.501(2) Å at 213 K). Interestingly, both of these distances are also longer than that in the hpp analogue (2.3167(6) Å at 213 K). Upon moving from hpp to tbn to tbo, the measured N–C–N angle of the guanidinate ligand increases by approximately 9º for each ligand. It is clear that an increase in the bite angle does not lead to the same increase in the bond length between Ru atoms. While the increase in Ru–Ru distance is 0.06 Å between the corresponding hpp and tbn compounds, it doubles to 0.12 Å for the tbn and tbo analogues. This significant increase presumably affects the bonding orbital occupancies (vide infra).

It should also be noted that the structure of **1** measured at 30 and 213 K show no perceptible change in bond distances, suggesting that there is only one electronic configuration over the temperature range. Similarly for **2** measurements at 30, 70 and 213 K show no noticeable structural differences, and again, the invariability of the structure is consistent with a single electronic configuration. What is not clear from these measurements is what the electronic configuration is since the magnetic properties are quite different for two compounds.

Magnetism. Because compounds with Ru_2^{6+} cores, which have ten electrons occupying the metal-based molecular orbitals, have been characterized with 0, 2, or 4 unpaired electrons,[2] magnetic susceptibility measurements, as well as variable temperature structural parameters, are essential to provide insight into the electronic configuration. The room temperature χT value of 0.9 emu·K·mol^{-1} for **1**, shown in Figure 2, is consistent with the presence of two unpaired electrons, as was the case for $Ru_2(hpp)_4Cl_2$.[14] Similarly to $Ru_2(hpp)_4Cl_2$, the magnetism gradually diminishes as the temperature is reduced and the χT value is essentially zero at 2 K. These magnetic and structural data support an electronic configuration of $\sigma^2\pi^4\delta^2\pi^{*2}$ in which the low temperature diamagnetism may be interpreted as a consequence of a large zero-field splitting (ZFS). This is further supported by modeling the magnetic data that yields values of $g_{(iso)}$= 2.01, D = 261 cm^{-1}, consistent with the earlier work.[2,14] The equation utilized for the fitting was

$$c = \frac{Nb^2g^2}{kT} \cdot \frac{\left(e^{-D/kT} + \left(\frac{2kT}{D} \right) \left(1 - e^{-D/kT} \right) \right)}{\left(1 + 2e^{-D/kT} \right)} \qquad \textbf{(1)}$$

where D is the ZFS parameter, k is the Boltzmann constant, N is Avogadro's number, and ß is the Bohr magneton. The ZFS parameter for **1** is the highest yet seen for a Ru_2^{6+} guanidinate compound, but matches well with other diruthenium compounds, as shown in Table 4.

In contrast **2** is essentially diamagnetic at ambient temperature.[27] The difference in magnetic behavior relative to **1** indicates that the electronic structure must be different and is consistent with the large difference in Ru–Ru distances (vide supra). However, this does not answer the question as to what the electronic structure of **2** would be.

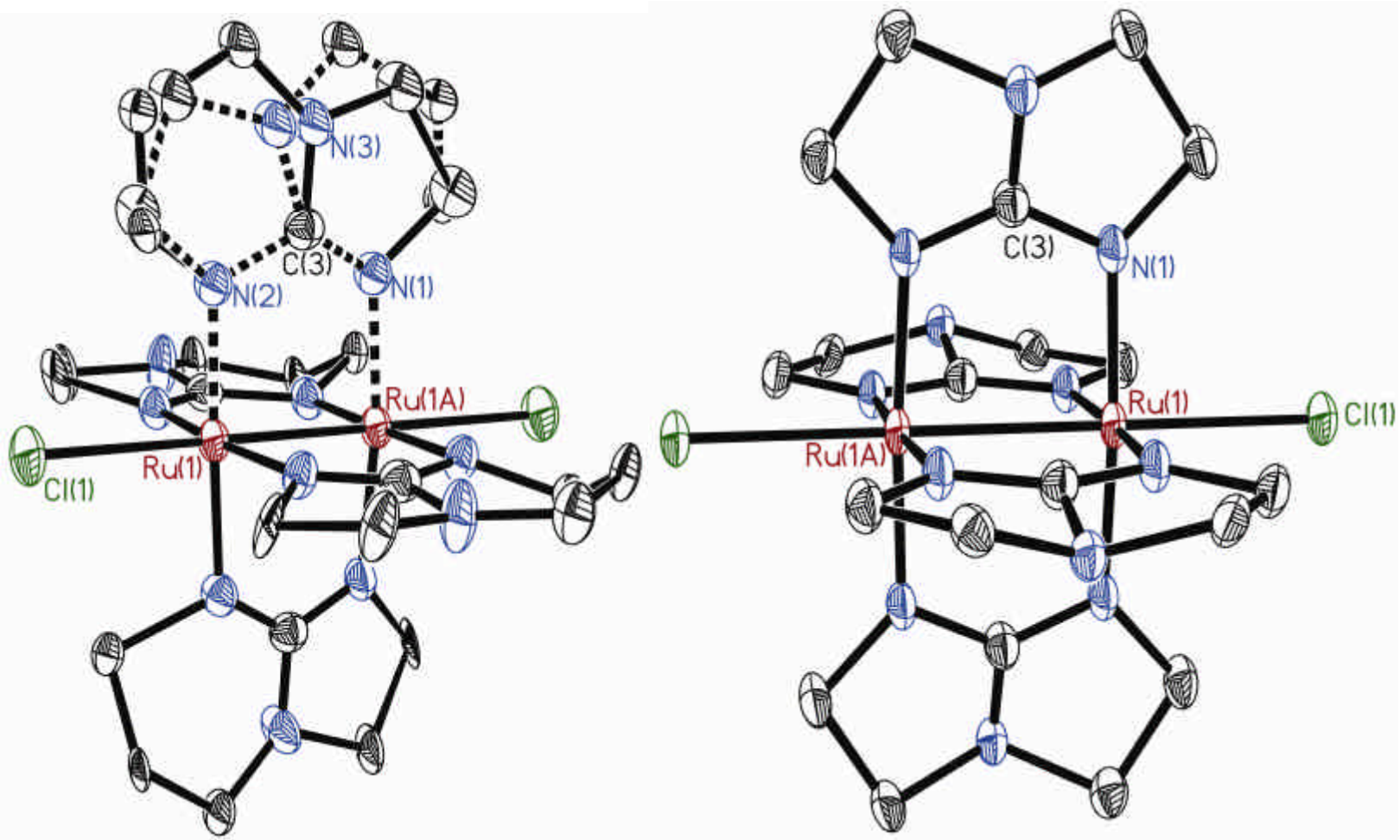

Figure 1. The molecular structures of **1** and **2,** shown as thermal ellipsoids at the 30% probability level. The two orientations of the ligand in **1** are due to the asymmetric rings in a tetragonal space group. Hydrogen atoms are omitted for clarity.

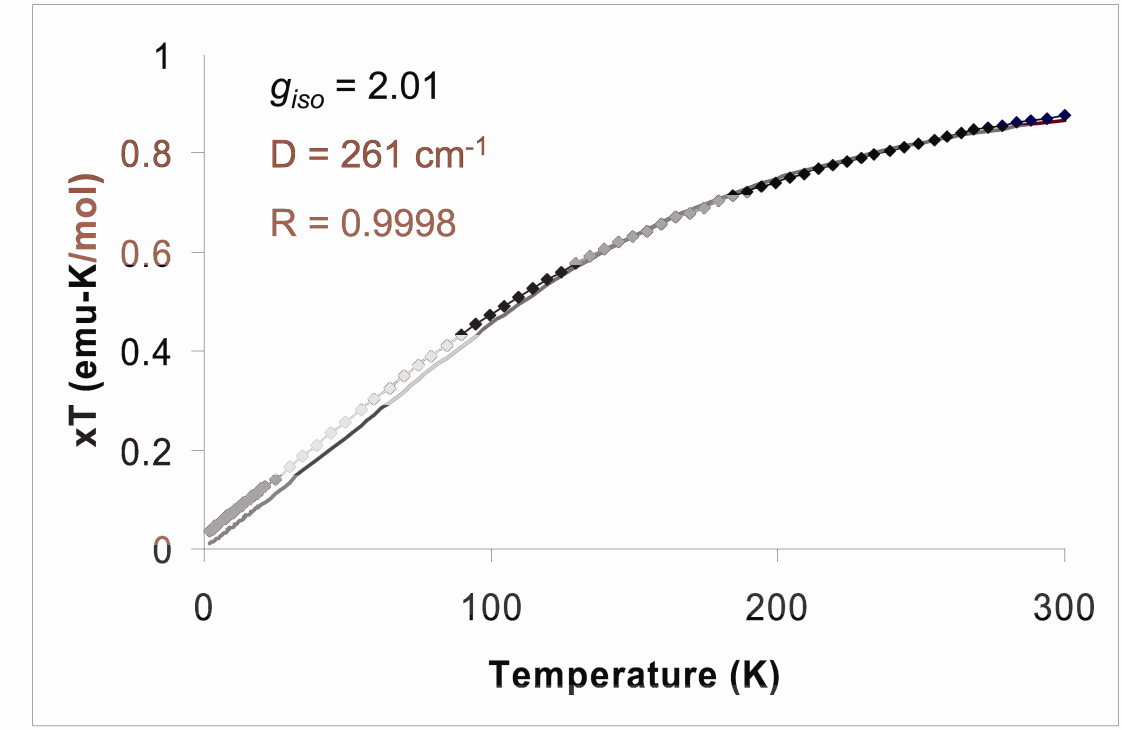

Figure 2. The temperature dependent magnetic susceptibility of **1**. The squares represent experimental values and the solid line the fitting of these experimental data. The inset shows the fitting parameters. There are two unpaired electrons at ambient temperature but a large zero-field splitting makes the compound appear as essentially diamagnetic at about 2 K.

Table 4. Large zero-field splitting parameters in diruthenium compounds.

Compound	D (cm^{-1})	Reference
1	261	This Work
$Ru_2(hpp)_4Cl_2$	227	14
$Ru_2(hpp)_4(O_3SCF_3)_2$	242	14
$Ru_2(O_2CCH_3)_4$	244	16b
$Ru_2(O_2CC_6H_5)_4(H_2O)_{1.2}(C_2H_5OH)_{0/8}$	215	16b

Computational Studies. Density functional theory (DFT) calculations were employed to provide a possible explanation of the observed diamagnetism of **2** and offer insight into the possible electronic structure. These DFT[28] calculations were performed

with the hybrid Becke's[29] three-parameter exchange functional and the Lee-Yang-Parr[30] non-local correlation functional (B3LYP) in the Gaussian 03 program.[31] Double-? quality basis sets (D95)[32] were used on C, N and H atoms as implemented in Gaussian. Correlation consistent double-zeta basis sets (CC-PVDZ)[33] were applied for the O atoms. A small effective core potential (ECP) representing the 1s2s2p3s3p3d core was used for the ruthenium atoms along with its corresponding double-? basis set (LANL2DZ).[34] All calculations were performed on either Origin 3800 64-processor SGI or Origin 2000 32-processor SGI supercomputers located at the Texas A&M supercomputing facility.

Calculations were performed for both **2** and the cation $Ru_2(tbo)_4^{2+}$, using the parameters from the crystal structure as a starting geometry. The orbital ordering diagram created using the calculations is shown in Figure 3. The calculated energies for the dication species indicate that it is the guanidinate ligands themselves that destabilize the σ bonding orbital, which becomes higher in energy than the π bonding orbitals. When interactions with the axial chlorine atoms are included in the calculation, the σ bonding orbital is further raised in energy, such that it becomes the LUMO, above the π, π^* and δ orbitals. Using the results of the calculations the energies for the π, π^*, δ and σ orbitals can be assigned as shown in Figure 4. These energies yield an electronic configuration of $\pi^4\pi^{*4}\delta^2$, and a total bond order of one. Because the only net metal–metal bonding arises from a δ^2 interaction, the bond is expected to be weak. The long Ru–Ru bond length in **2** is consistent with this description. It should be noted that this

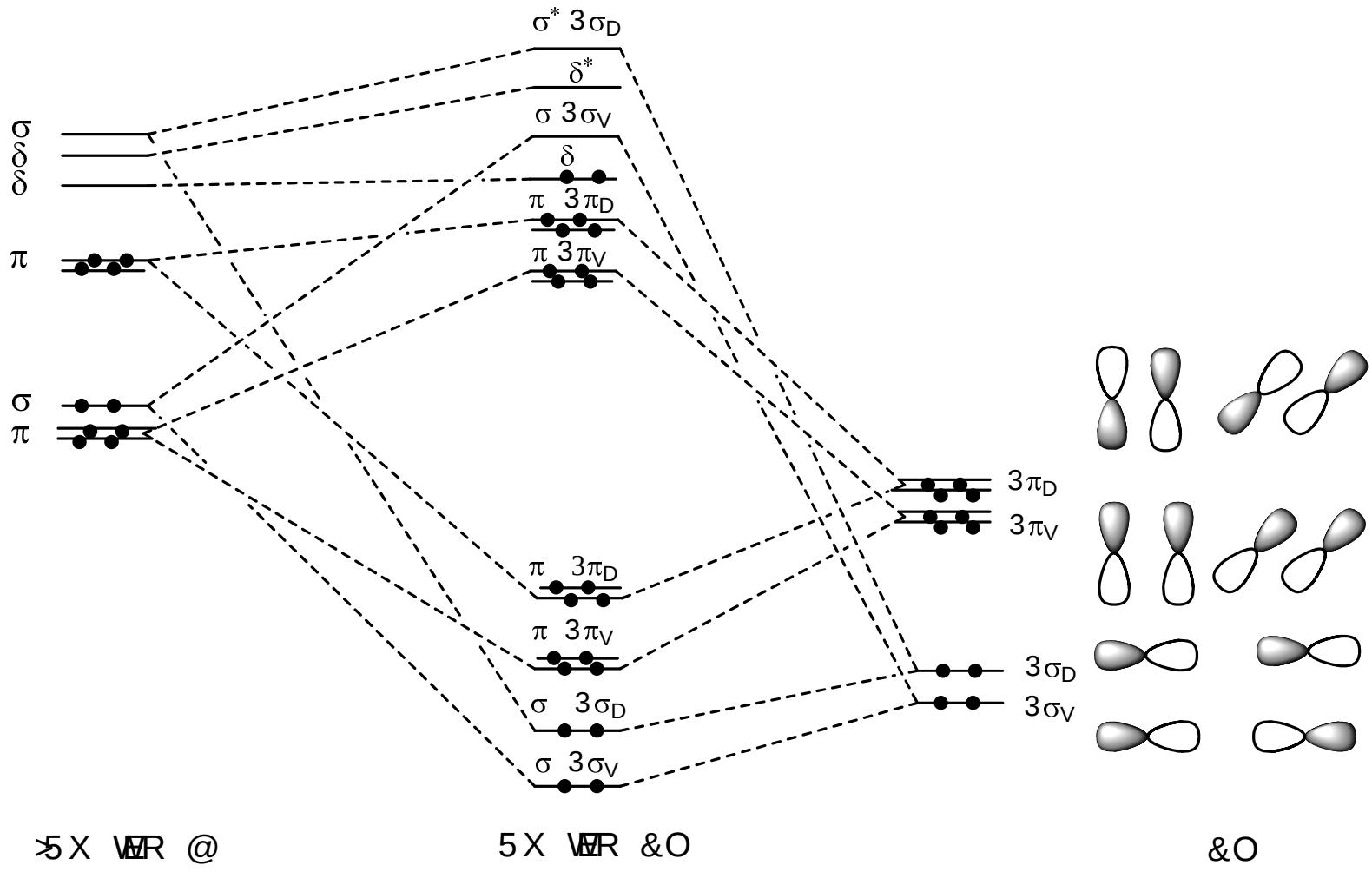

Figure 3. Qualitative molecular orbital energy diagram for **2** and the corresponding $[Ru_2(tbo)_4]^{2+}$ cation.

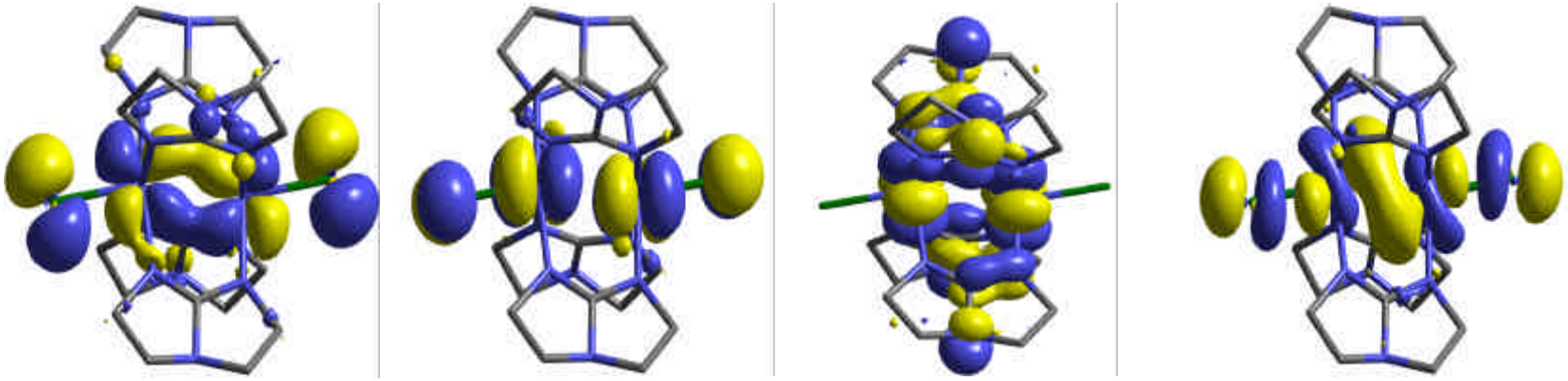

Figure 4. Metal-based molecular orbitals for **2** from DFT calculations. The d interaction provides the only metal–metal bond.

electronic configuration is reminiscent of that of $\pi^4\delta^2\pi^{*4}$ proposed for [Ru_2^{6+}] compounds with strong σ donating axial ligands.[5,6,7] Ligands such as –C=N and –C=CR interact with the d_{z2} orbitals of the Ru atoms, raising their energy and resulting in an electronic configuration of $\pi^4\delta^2\pi^{*4}$. While Cl^- is by no means a strong σ donor, it may interact with the metal atoms to a sufficient amount that, when combined with the divergent bite angle of the tbo ligand, causes a change in the electronic configuration as has been found in $W_2(hpp)_4Cl_2$.[35]

Conclusions

It has been shown that for Ru_2^{6+} species spanned by guanidinate ligands significant changes in electronic and magnetic properties can be induced by modification of ligands. The electronic structure $Ru_2(tbn)_4Cl_2$ is $\sigma^2\pi^4\delta^2\pi^{*2}$ while that in $Ru_2(tbo)_4Cl_2$ is $\pi^4\pi^{*4}\delta^2$. As a consequence of the changes in configuration **1** is paramagnetic at ambient temperature while **2** is diamagnetic, consistent with the DFT calculations. The underlying cause of the different electronic configurations is the ligand bite angle. The donor orbitals of the tbo ligand push the ruthenium atoms apart to such an extent that there is a change in the orbital energies, leading to a lower bond order and an increase in the metal-to-metal bond distance.

CHAPTER III

A BETTER UNDERSTANDING OF THE BONDING IN THE RARE Os_2^{7+} SPECIES

Introduction

Since the discovery of the first species with an unsupported quadruple bond having D_{4h} symmetry about four decades ago[1] emphasis in the search for analogous compounds have provided a wealth of them most of which have bridging ligands and a paddlewheel structure.[3] Common ligands employed to span the dimetal unit have been carboxylates and formamidinates. With very few exceptions the M_2^{n+} cores in these compounds have formal charges, *n*, of 4, 5 and 6. Rare examples of compounds structurally characterized having lower oxidation numbers and tetragonal paddlewheel structures are those containing V_2^{3+} units[36] as well as a few compounds with trigonal paddlewheel structures having M_2^{3+} units, M = Fe[37] and Co.[38]

More recently it has been found that bicyclic guanidinate ligands can stabilize dimetal units with unique characteristics. A notable example is that with M_2^{4+} units, M = Mo,[39] W,[40] spanned by four hpp ligands (hpp = the anion of 1,3,4,6,7,8-hexahydro-*2H*-pyrimido[1,2-*a*]pyrimidine). These compounds are so easily oxidized that the oxidation potentials are at least 1.5 V lower than for the formamidinate or carboxylate analogues of molybdenum.[41] Furthermore the ionization potential of $W_2(hpp)_4$ is lower than those of cesium,[42] the textbook example of a stable element with the lowest known ionization

energy.[43] The main reason for stabilization of the high oxidation states by these bicyclic ligands is the destabilization of the d orbitals of the quadruply bonded unit because of a strong interaction with the pp orbitals of the ligand.[44] It should be noted that guanidinate ligands can also stabilize, to some extent, high formal oxidation states in mononuclear compounds and this type of ligands have become increasingly important in coordination chemistry.[45]

Because of the ability of these bicyclic ligands to stabilize high oxidation numbers efforts have been made to explore the chemistry of paddlewheel complexes with such ligands and a series of compounds with M_2^{6+} cores have since been made.[46] More importantly in 2003, the first species with an M_2^{7+} core were isolated and structurally characterized and these results published in a preliminary communication for two solvates of $[Os_2(hpp)_4Cl_2]PF_6$, **3**, one having interstitial hexane and the other one acetone molecules.[47] As the oxidation state of the dinuclear unit increases the metal based orbitals are expected to contract which should diminish the orbital overlap leading to metal–metal bond formation. An additional question that is raised upon oxidation is whether the lost electron is removed from a mainly metal-based orbital or a ligand-based orbital. Thus there is a question as to whether the oxidation of the diamagnetic species $Os_2(hpp)_4Cl_2$, truly lead to an Os_2^{7+} core, or if the process is simply oxidation of the guanidinate ligand. One of the few experimental techniques capable of differentiating between these two possibilities is EPR spectroscopy since a ligand-based oxidation would be expected to yield an organic radical giving a spectrum with a sharp signal and a g value very close to that of the free electron (g = 2.00)[48] but a metal-based oxidation

would generally provide *g* values different from the free electron because of the interactions with the transition metal orbitals. Our early studies of this species done using powdered crystalline samples provided EPR spectra having an extraordinarily broad signal with a line width of ~6000 G and a very low *g* of 0.791±0.037.[47] This is consistent with a metal-based oxidation as is the decrease in Os–Os distance from 2.379(2) to 2.3309(4) in **1**·2acetone or 2.3290(6) Å in **1**·hexane. However, the rather broad and low value of *g* in the EPR spectra remained poorly understood.

To provide further insight on the properties of this system we have now reinvestigated the magnetic properties of these species by carefully re-measuring the EPR spectra not only in powder crystalline samples but also using frozen solutions and single crystals. It should be noted that since the Os_2^{7+} units contain nine metal-based electrons, the electronic configuration is expected to be $s^2p^4d^2d^*$ or perhaps $s^2p^4d^2p^*$ if the energy of the p* orbitals is lower than that of the d* orbitals as is often the case in Ru_2^{5+} species.[9]

Experimental

All syntheses were carried out under an inert atmosphere using standard Schlenk techniques, unless otherwise noted. Solvents were dried using a Glass Contour solvent system. $[Os_2(hpp)_4Cl_2](PF_6)$, **3**, was prepared according to the literature. Briefly, a flask was charged with 0.200 g (0.200 mmol) of $Os_2(hpp)_4Cl_2$ and 0.038 g (0.201 mmol) of $FcPF_6$. 20 mL of methylene chloride were added to the solid mixture, immediately producing a deep purple solution. After the solution had been stirred for thirty minutes, the solvent was removed by vacuum. The residue was washed by ether (2 x 10 mL),

after which it was dissolved in acetone. This solution was then filtered through a frit with Celite and layered with hexanes to produce crystals of **3**·2acetone. Crystals of **3**·hexane were obtained by dissolving a sample of **3**·2acetone in methylene chloride and layering the solution with hexanes.

The X-band (~9.5 GHz) EPR data of powders, frozen glass and single crystal were recorded on a Bruker E500 spectrometer. Precise temperature control to 4 K was obtained by utilizing an Oxford continuous flow liquid He cryostat. The magnetic field was calibrated with the DPPH radical (g = 2.0037) and a built in NMR teslameter. The frequency was monitored with a digital frequency counter. Powder samples were prepared by crushing crystalline material and placing the sample under vacuum overnight. The frozen glass samples were prepared by dissolving the crystalline material in methylene chloride. Angle dependence data were obtained with use of a single axis goniometer attached to the sample tube.

X-ray Structure Determination. Data were collected on a Bruker SMART 1000 CCD area detector system. Cell parameters were determined using the SMART software suite.[49] Data reduction and integration were performed with the software SAINT.[50] Absorption corrections were applied by using the program SADABS.[51] The positions of the Os atoms were found via direct methods using the program SHELXTL.[52] Subsequent cycles of least-squares refinement followed by difference Fourier syntheses revealed the positions of the remaining non-hydrogen atoms. Hydrogen atoms were added in idealized positions. All hydrogen atoms were included in the calculation of the structure

factors. All non-hydrogen atoms were refined with anisotropic displacement parameters. An Oxford Helium Cryostat was used to obtain a low sample temperature.

Results and Discussion

Structural Considerations. Before a discussion of the EPR data is important to summarize the structural features obtained from X-ray crystallography from two solvates.[47] In both **3**·2acetone and **3**·hexane, the $[Os_2(hpp)_4Cl_2]^+$ cations are structurally very similar and have a paddlewheel structure, as shown in Figure 5. The former crystallizes in the orthorhombic space group *P*nma (Z = 4) with dimetal units having idealized D_{4h} symmetry while the latter has strict crystallographic D_{4h} symmetry since it crystallizes in the tetragonal space group *P*4/mbm with *Z* = 2, and the Os–Os bonds are parallel to the unique *c* axis. In both of these compounds the Os–Os distances are chemically indistinguishable (2.3309(4) in **3**·2acetone and 2.3290(6) Å in **3**·hexane) and about 0.05 Å shorter than that in the precursor $Os_2(hpp)_4Cl_2$ (Os–Os distance = 2.379(2) Å).[53] The structure of **3**·2acetone was obtained at 30 K to ensure that the EPR signals arising at low temperatures could be accurately described in terms of the molecular structure. The structure at 30 K matches that of 213 K, with an Os-Os distance of 2.3231(14) Å. A comparison of the crystallographic information for the structures at different temperatures is given in Table 5.

Table 5. Comparison of **3**·2acetone structures at 213 and 30 K.

	30 K	*213 K*
Space group	Pnma	Pnma
a (Å)	17.206(10)	17.282(2)
b (Å)	25.165(15)	25.425(2)
c (Å)	9.994(6)	10.1454(9)
Z	4	4
Os-Os (Å)	2.3231(14)	2.3309(4)
Os-Cl (Å)	2.509(2)	2.5199(13)

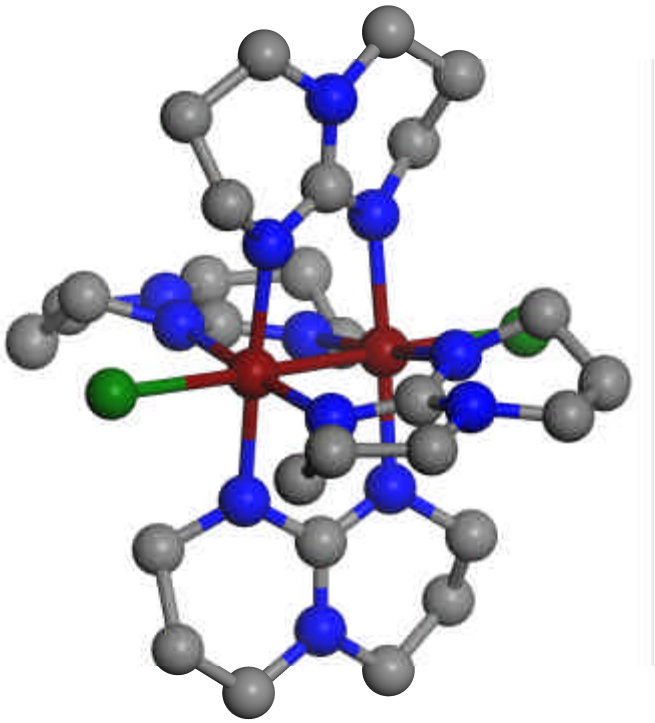

Figure 5. A structural representation of the cation of **3**. Hydrogen atoms are omitted for clarity.

EPR Results. As mentioned in the Introduction, EPR spectra of **3** showing a broad signal and a very low *g* of 0.791±0.037 were obtained using solid samples.[47] Broad bands are sometimes associated with solid state effects such as interactions between chains.[54] To aid in the understanding of these spectra, it was considered essential to confirm whether the spectra truly represented those of the product by using crystalline samples as the source of **3** in all studies. It was also considered vital to remove intermolecular effects to disentangle potentially overlapping peaks. To resolve these potential peaks, and to obtain more accurate *g* values, the EPR spectra of a frozen glass sample were obtained. At low temperatures, two clear signals are seen, shown in Figure 6. The simulated *g* values are 1.383 ± 0.004 and 0.620 ± 0.002. These signals disappear when the temperature is raised above 30 K. Although these values are extremely low, they are the actual *g* values, as this is an m_s = ½ system. With these low values and the exceptionally large gap (~0.8) between the *g* values, any doubt that the oxidation takes place on the metal atoms rather than the ligands seems misplaced. The average *g* value obtained from these spectra is 0.880, a fairly significant deviation from the average value given by the powder samples. It must be concluded that the powder samples used were not completely uniform, yielding spectra with incorrect *g* values. That multiple peaks are present in the powder spectra speaks to this. Additional information can be gleamed from the frozen glass spectra. That only two signals, $g_{\|}$ and $g_{\perp}$, are seen indicates that the molecule retains its axial symmetry at these temperatures.

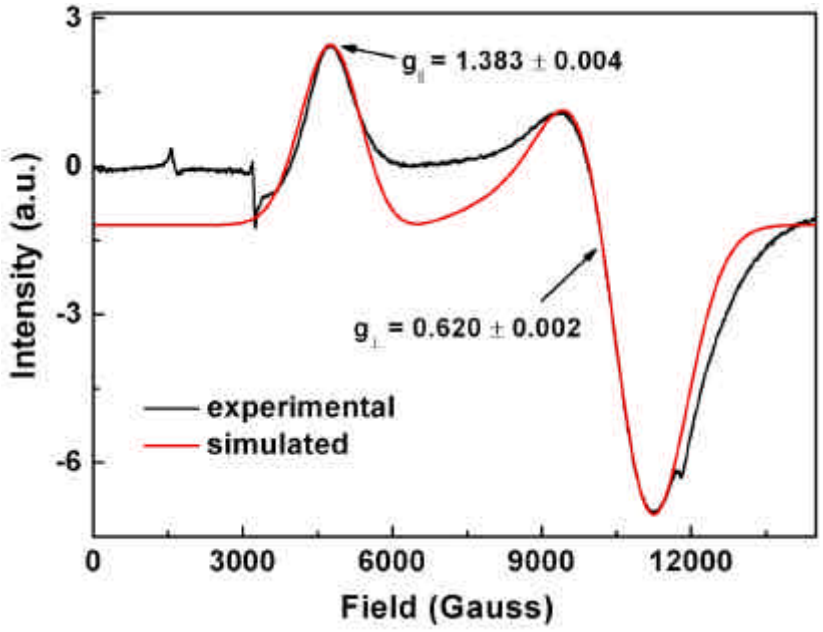

Figure 6. (a) EPR spectra of a frozen glass sample of **3** in CH_2Cl_2 from 4 to 50 K and (b) a simulated spectrum.

While both the EPR spectrum and **3** have axial symmetry, it was considered necessary to determine the orientation of the *g* vectors relative to the molecule. This requires the observation of the angular dependence of the two signals as a single crystal is rotated about an axis. The ideal candidate for this experiment would be **3**·hexane, owing to its tetragonal unit cell. Unfortunately, no crystal of **3**·hexane could be found that was large enough to produce a clear EPR spectrum. However, a plate crystal of **3**·2acetone was found to produce a well resolved spectrum. This solvate crystallizes in a group of lower symmetry, Pnma, but as an orthorhombic group it maintains a high enough degree of symmetry to be useful. While the molecules do not align perfectly with the edges of the unit cell, the angle of the Os-Os bonds from the unit cell edges is

only approximately 8°. This small deviation means that the differences arising from a change in alignment of the Os-Os bond will be readily apparent.

For this experiment, the short axis of the plate crystal was set perpendicular to the magnetic field, shown in Scheme 3a. The angular dependence of the signal intensities as the crystal was rotated in the magnetic field is provided in Figure 7. The intensity of the two *g* signals do indeed rise and fall as the crystal is rotated a total of 180°. The spectra have been arranged so that the spectrum with the most intense peak at ~4800 gauss was set at 0°. When looking at the spectrum labeled 90°, the peak at 4800 gauss has nearly disappeared and only the peak at ~9000 gauss is visible. That these two extremes are 90° apart is consistent with the orthorhombic unit cell. A spectrum was also obtained with the short axis parallel to the magnetic field (Scheme 3b), shown in Figure 8. This spectrum matches well with the 0° spectrum; that is, both spectra are at a limit where the 4800 gauss signal is strongest. However, it should be noted that both peaks are still present at this alignment and in the 0° spectrum, as observed when comparing them to the frozen solution sample.

Scheme 3. (a) The plate of **3**·2acetone is rotated perpendicular to the magnetic field and (b) set with face in-line with the magnetic field.

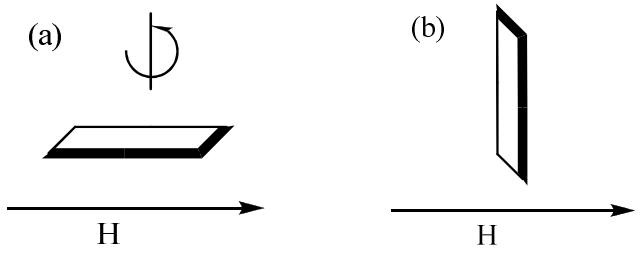

Crystal facing has identified the plane perpendicular to the short axis (that is, the top of the plate) as the 1i0 *hkl* plane. With this information, the EPR data can be fully explained. The Os-Os bonds are 62.8° out of the 1i0 plane. At this orientation, both $g_{\parallel}$ and $g_{\perp}$ peaks would be expected to be observed when that plane is placed perpendicular to the magnetic field, as indeed they are. Placing the 1i0 plane parallel to the field will yield differing intensities as the unit cell is rotated, as there is still a mixture of alignments. A special situation occurs when the *ab* plane of the cell is perpendicular to the field. At this position, all of the Os-Os bonds are nearly perpendicular to the field diagramed in Figure 9. As no other rotational alignment of the crystal will yield such an ordering to the magnetic field (parallel or perpendicular), this position will correspond to the point where the average *g* value most closely approaches one of the two frozen glass values (1.4 vs. 0.6). This is seen at the 90° spectrum in Figure 7, where the approximate *g* value of 0.7 means that this orientation of the Os-Os bond (that is, perpendicular to the magnetic field) corresponds to $g_{\perp}$.

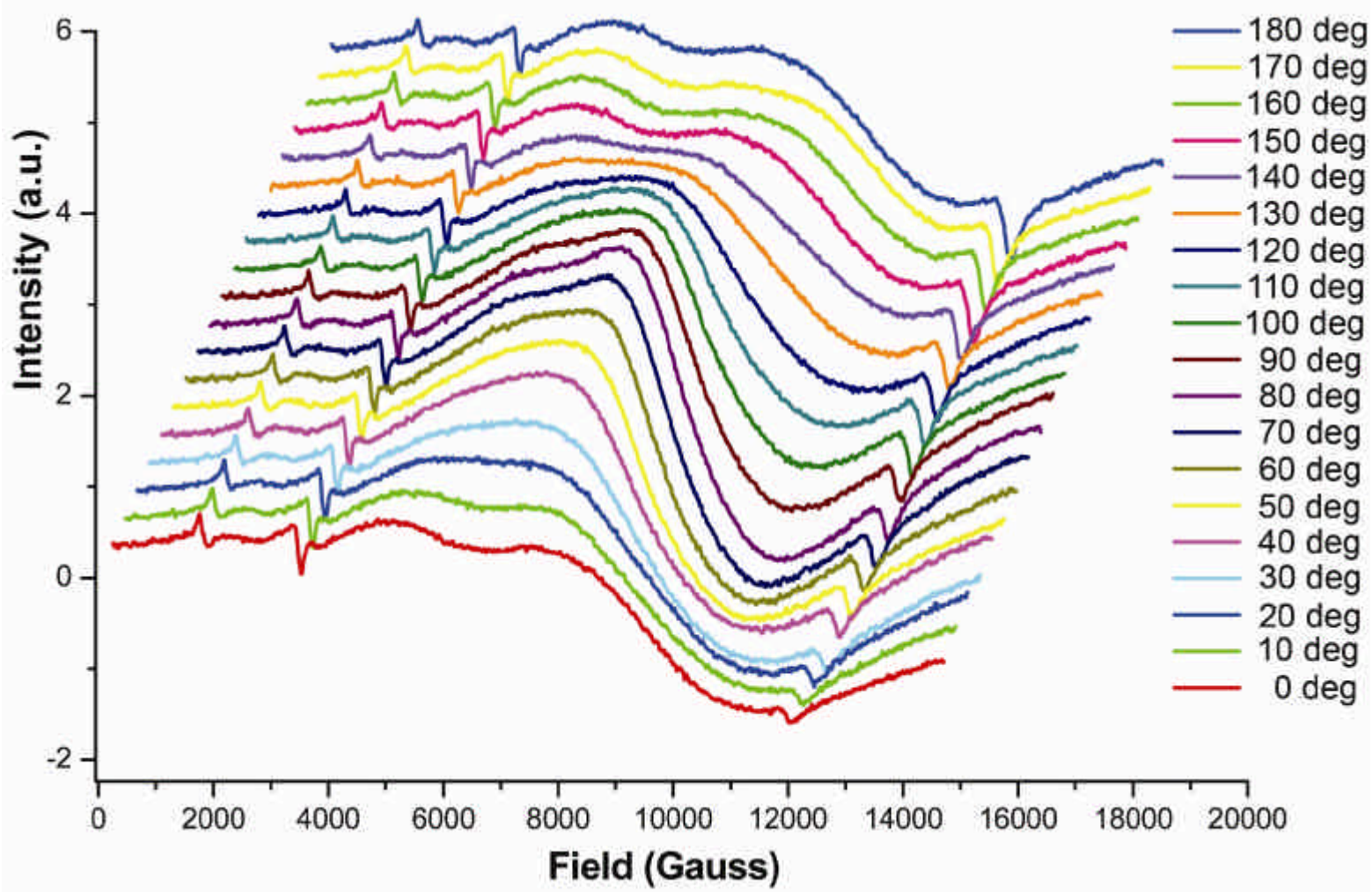

Figure 7. Angle dependent X-band EPR spectra of **3**·2acetone plate crystal.

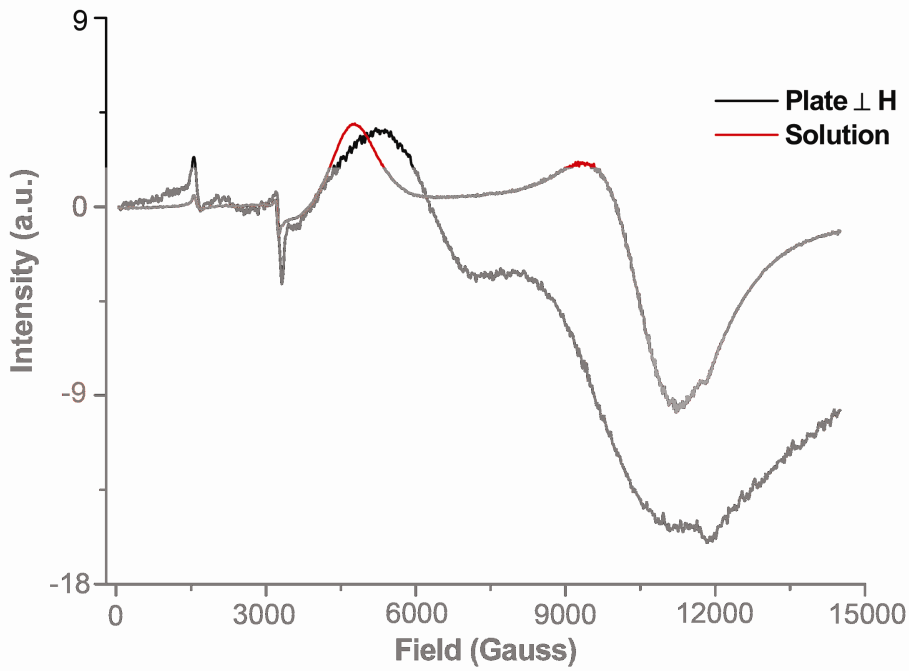

Figure 8. EPR spectrum of the **3**·2acetone plate set perpendicular to the magnetic field. The frozen solution spectrum at 6 K is included for comparison.

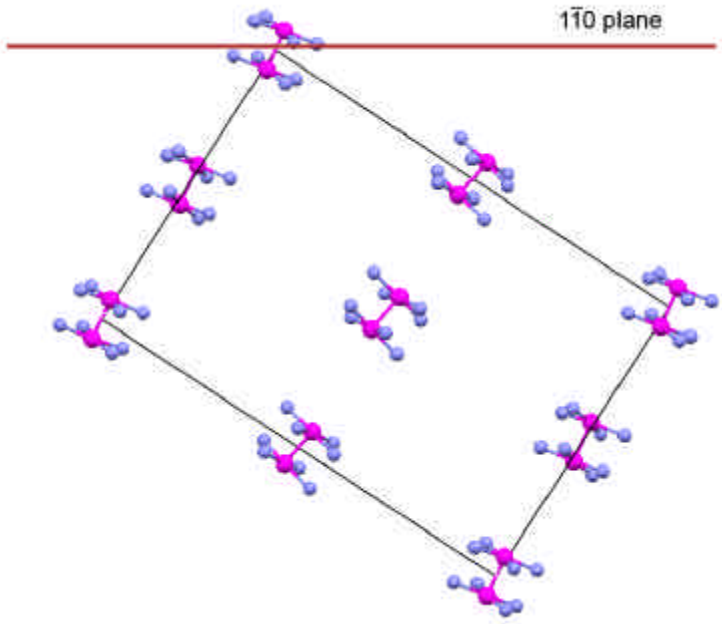

Figure 9. A view of the *ab* plane of the **3**·2acetone unit cell. This orientation shows how the Os-Os bonds can be perpendicular to the magnetic field.

With this information, it is now possible to determine the direction of the *g* vectors. Owing to the high symmetry of the molecule, polar angles are the best descriptors of the vectrors. As $g_{\perp}$ has been identified as being perpendicular to the Os-Os bond, $g_{\parallel}$ (or g_{zz}) is assigned to lie along the metal-metal bond. While the value of $g_{\perp}$ is equal in all directions about the Os-Os bond, g_{xx} and g_{yy} are assigned to create a right-handed Cartesian system when pointed in the directions of the coordinating nitrogen atoms, diagramed in Figure 10. With these assignments made, the value of *g* along each unit cell direction can be calculated, with $g_a = 1.483$, $g_b = 0.815$, and $g_c = 0.825$.

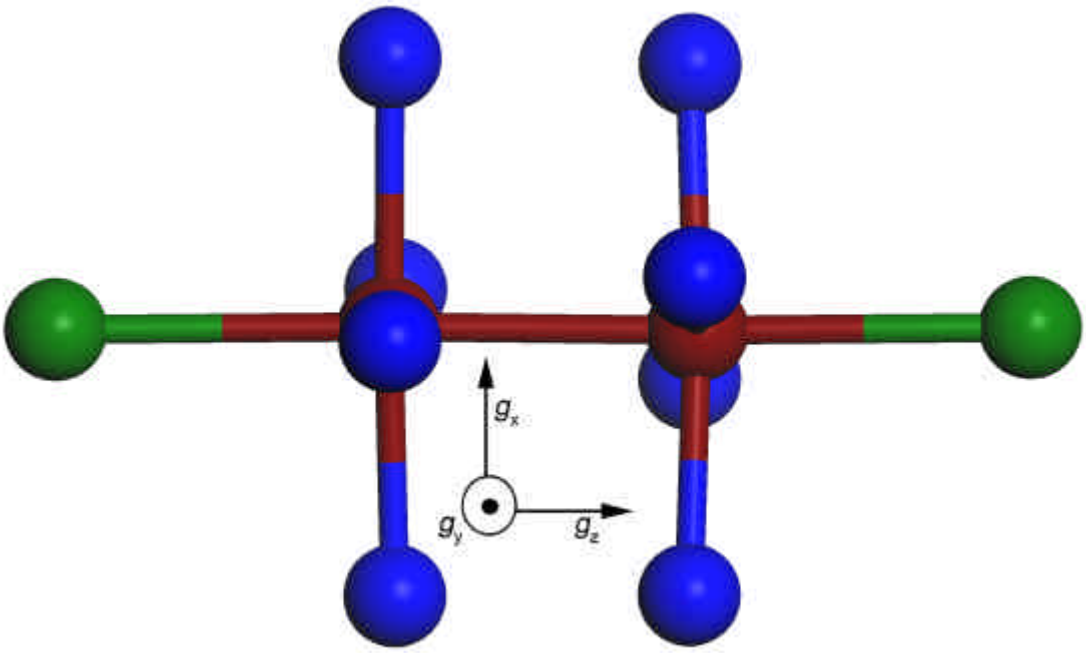

Figure 10. View of the *g* tensor principle axes in **3**. g_z is along the Os-Os bond, while g_x and g_y are directed towards the coordinating nitrogen atoms. Atoms not coordinated to the osmium atoms are omitted for clarity.

Implications to Electronic Structure. The EPR data unambiguously support that the unpaired electron in **3** is in a metal-based orbital and thus verify that oxidation of $Os_2(hpp)_4Cl_2$ leads to an Os_2^{7+} unit. Since there are nine metal-based electrons in **3**, one of the electrons is an antibonding orbital and thus the formal bond order in the dimetal unit is 3.5. There is however some uncertainty as to whether the electronic configuration either $s^2p^4d^2d^*$ or $s^2p^4d^2p^*$ since the relative energy of these orbitals may vary in some dimetal species such as those containing Ru_2^{5+} units which until recently has been commonly been referred as having an electronic configuration of the type $s^2p^4d^2(d^*p^*)^3$ because of the ambiguity of where the antibonding electrons are located.[55]

For the diosmium system, it is known that the electronic configuration for the precursor of **3** is $s^2p^4d^2d^{*2}$ since this molecule is diamagnetic.[53] Furthermore removal of one electron from this precursor reduces the Os–Os distance by about 0.05 Å. This bond shortening is not only consistent with removal of an electron in an antibonding orbital but the magnitude is in the range commonly observed when an electron from a d orbital is removed form a dimetal units such as those having Mo_2^{4+} units.[56] These results strongly support the assignment of an electronic configuration of $s^2p^4d^2d^*$ for **3**.

Conclusions

Additional studies have been performed on the molecule $[Os_2(hpp)_4Cl_2](PF_6)$, focusing on the use of EPR spectroscopy to probe the electronic properties of this compound. The frozen glass spectra obtained show remarkably low values for $g_{\|}$ and $g_{\perp}$, as well as a large separation between the two. The electronic configuration is determined to be $\sigma^2\pi^4\delta^2\delta^*$, with the oxidation being metal based. Finally, the vector

components of the *g*-tensor are identified and the value of *g* along each unit cell edge determined.

CHAPTER IV

FURTHER STUDIES OF RELATED Re_2^{6+} AND Re_2^{7+} SPECIES WITH DIVERGENT BICYCLIC GUANIDINATE LIGANDS

Introduction

The chemistry of dirhenium compounds is among the richest of all metal-to-metal bonded species.[57] Beginning with the halides,[1] a wide range of ligands have been used to create complexes with multiple bonds between two rhenium atoms, including carboxylates,[58] sulfates,[59] phosphates,[60] and hydroxypyridinates,[61] among others. Used with rhenium, these compounds paved the way to the first structurally confirmed metal-to-metal bond quadruple bond,[1] and the first dimetal triple bond.[62]

Bicyclic guanidinate ligands, primarily hpp (the anion of 1,3,4,6,7,8-hexahydro-*2H*-pyrimido[1,2-*a*]pyrimidine), have been used with great effect over the last decade to open the doors for the possibility of dimetal species with rare or otherwise unprecedented oxidation states outside the usual range of M_2^{n+}, n = 4, 5 and 6 .[63] Now that a vast survey of the transition series has been completed using hpp,[3] this chemistry is being expanded by a variety of new bicyclic guanidinate ligands. One area of focus has been in improving the solubility of these compounds, which has been accomplished with the use of two alkyl-substituted ligands, TMhpp (the anion of 3,3,9,9-tetramethyl-1,5,7-triazabicyclo[4.4.0]dec-4-ene) and TEhpp (the anion of 3,3,9,9-tetraethyl-1,5,7-triazabicyclo[4.4.0]dec-4-ene).[18] The other focus is the use of differing ring sizes in

these ligands to adjust the metal-to-metal bond distance and thus 'tweak' the electrochemical properties of these compounds.[64] Cyclic voltammetry has proved an effective tool to probe the electronic character of a particular species, in part to its ability to identify with reasonable clarity the reversibility of redox processes. In the case of dirhenium guanidinate compounds this is an important tool to use, given the ability of guanidinate ligands to shift oxidation potentials far towards lower values.[41]

In this study several new dirhenium guanidinate compounds are prepared and characterized by X-ray diffraction and electrochemical measurements. The effects of both the bridging ligands and axial ligands on the structural and electrochemical properties are examined. Several oxidized species are also prepared to elucidate how differences in the bridging ligands are manifested in their electronic structures.

Experimental

All syntheses were carried out under inert atmosphere using standard Schlenk techniques unless otherwise noted. The starting materials $(NBu_4)_2Re_2Cl_8$, ferrocenium hexafluorophosphate, and silver triflate were purchased from Sigma-Aldrich and used as received. $Re_2(hpp)_4(O_3SCF_3)$,[65] Htbn, and Htbo[64] were prepared according to the literature. Ferrocenium triflate was prepared by reaction of silver triflate with ferrocene, and purified by recrystallization from acetone. Solvents were dried using a Glass Contour solvent system. Mass spectrometry data (electrospray ionization) were recorded at the Laboratory for Biological Mass Spectrometry at Texas A&M University, using an MDS Series Qstar Pulsar with a spray voltage of 5 kV. Infrared spectra were recorded in a Perkin-Elmer 16PC FT IR spectrophotometer as KBr pellets. Electronic spectra were

recorded on a Shimadzu UV-2501 PC spectrophotometer. The cyclic voltammograms (CVs) were taken using a CH Instruments Model-CH1620A electrochemical analyzer in 0.1 M Bu_4NPF_6 solution in CH_2Cl_2 with Pt working and auxiliary electrodes, Ag/AgCl reference electrode, and a scan rate of 100 mV s^{-1}. All potentials are referenced to the Ag/AgCl electrode.

Synthesis of $Re_2(tbn)_4Cl_2$, 4. To a flask charged with 200 mg (0.170 mmol) of $(Bu_4N)_2Re_2Cl_8$ in 20 mL of THF was added a solution of Li(tbn) (0.7 mmol) in THF. The mixture was refluxed overnight, during which a violet precipitate was formed. This precipitate was collected on a fritted filter and washed with THF (2 × 5 mL). Yield: 100 mg (61 %). Crystals were grown by dissolving the compound in CH_2Cl_2 and layering with hexanes. Mass Spec.: Calcd $(M\text{-}Cl)^+$: 905 amu. Found: 905 amu. IR: 3150 (w), 2970 (m), 2849 (m), 1563 (s), 1515 (s), 1451 (m), 1121 (m). UV-vis: 567 nm (λ_{max}), 411 nm (shoulder). ^1H NMR ($CDCl_3$): 3.55 ppm (mult., 8 H); 1.97 ppm (p, 2 H).

Synthesis of $Re_2(tbo)_4Cl_2$, 5. To a flask charged with 200 mg (0.170 mmol) of $(Bu_4N)_2Re_2Cl_8$ in 30 mL of propionitrile was added a solution of Li(tbo) (0.70 mmol) in 15 mL of THF. The mixture was refluxed overnight, during which a brown precipitate was formed. This precipitate was collected on a fritted filter and washed with THF (2 × 5 mL). Mass Spec.: Calcd $(M\text{-}Cl)^+$: 849 amu. Found: 849 amu. IR: 2950 (m), 2900 (w), 1260 (s), 1110 (s), 1025 (s), 815 (s). UV-vis: 335 nm. ^1H NMR ($CDCl_3$): 3.929 ppm (t, 4 H); 3.422 (t, 4 H).

Synthesis of $[Re_2(tbn)_4Cl_2]Cl$, 6. In the course of characterizing **1**, a sample was left in a sealed NMR tube for approximately two weeks. During this time, the

solution in $CDCl_3$ changed from violet to brown, and several crystals formed on the tube walls which were identified as **3** through X-ray diffraction studies.

Synthesis of $[Re_2(tbn)_4Cl_2](PF_6)$, 7. To a flask charged with 100 mg (0.088 mmol) of $Re_2(tbn)_4Cl_2$ and 31 mg (0.093 mmol) of ferrocenium hexafluorophosphate were added 20 mL of methylene chloride. The resulting solution immediately turned very dark. After the solution was stirred for 30 min, the solvent was removed by vacuum. The residue was washed with ether (2 × 10 mL), and the remaining material was extracted with methylene chloride. Mass Spec.: Calcd $(M\text{-}PF_6)^+$: 940 amu. Found: 940 amu. IR: 3420 (w), 2930 (m), 2865(m), 1565 (s), 1370 (m), 1275 (m), 840 (s). UV-vis: 429 nm (λ_{max}), 576 nm.

Synthesis of $[Re_2(hpp)_4](O_3SCF_3)_3$, 8. To a flask charged with 50 mg (0.040 mmol) of $Re_2(hpp)_4(O_3SCF_3)_2$ and 15 mg (0.04 mmol) of ferrocenium triflate was added methylene chloride (20 mL). After the solution was stirred for 1 h, the solvent was removed under vacuum. The residue was washed with ether (2 × 10 mL), and the remaining solid was extracted with acetonitrile. Crystals were obtained from this dark green solution by layering with ether. The crystals were dark brown to reflected light. Mass Spec.: Calcd $(M\text{-}O_3SCF_3)^+$: 1222 amu. Found: 1222 amu. IR: 2963 (m), 2866 (w), 1380 (s), 1250 (s), 1228 (m), 1198 (s), 839 (m), 636 (m). UV-vis: 269 nm (λ_{max}), 356 nm, 451 nm, 601 nm.

X-ray Structure Determinations. Data were collected on a Bruker SMART 1000 CCD area detector system. Cell parameters were determined using the SMART software suite.[22] Data reduction and integration were performed with the software

SAINT.[23] Absorption corrections were applied by using the program SADABS.[24] The positions of the Re atoms were found via direct methods using the program SHELXTL.[25] Subsequent cycles of least-squares refinement followed by difference Fourier syntheses revealed the positions of the remaining non-hydrogen atoms. Hydrogen atoms were added in idealized positions. All hydrogen atoms were included in the calculation of the structure factors. All non-hydrogen atoms were refined with anisotropic displacement parameters.

Results and Discussion

Syntheses. Preparation of **4** and **5** followed the basic experimental procedure used for $Re_2(hpp)_4Cl_2$, where the lithium salt of the ligand was added to a solution of $(NBu_4)_2Re_2Cl_8$, as shown in Equation 2. The preparation of **5** followed that procedure with a slight modification; that is, a 2:1 mixture of propionitrile and THF was used to increase solubility and reduce the amount of incomplete ligand substitution that took place. For **4**, the increased solubility of the tbn ligand with respect to hpp allowed the use of only THF as the solvent without any significant loss of yield.

$$(Bu_4N)_2Re_2Cl_8 + 4Li(guanidinate) \longrightarrow Re_2(guanidinate)_4Cl_2 + 4LiCl + 2Bu_4NCl \quad \textbf{(2)}$$

Compound **6** was discovered serendipitously when crystals were observed in an NMR tube. A new spectrum was obtained using the tube, showing many broad peaks characteristic of a paramagnetic species. The structure was determined by use of X-ray diffraction. Though the NMR tube was sealed (J-Young), it is suspected that a small amount of oxygen was able to enter over time. The oxidation of dimetal guanidinates in

halogenated solvents has been well established.[66] In such cases, the newly formed cation of **3** abstracts a chloride from the $CDCl_3$ solvent, creating a neutral molecule and carbon radical.

Deliberate oxidation to Re_2^{7+} species **7** and **8** were carried out using the appropriate ferrocenium salt. The reactions proceeded swiftly and quantitatively, which was expected given the measured oxidation potentials for their respective Re_2^{6+} precursors (vide infra).

Structures. Crystallographic information for **4-6** and **8** are given in Table 6. Important bond lengths and angles may be found in Table 7. The structures of **4** and **5**, shown in Figure 10, display the typical paddlewheel arrangement found for dimetal species with four guanidinate ligands. Compound **4** crystallizes in space group *I*-4; unlike the analogous Ru_2^{6+} compounds, the tbn ligand is solved in only one orientation due to lack of an inversion center. Compound **5** crystallizes in space group *I*4/m. In this case, the only disorder present is in the non-coordinating nitrogen atom of the tbo ligand. The disorder was easily resolved by refining this atom over two positions, due to the puckering of the two five-membered rings.

Compound **1** has a Re–Re bond distance of 2.212(2) Å, which falls in the normal range for dirhenium(III) compounds containing a quadruple bond. The bond length in **5**, however, is among the longer distances measured for quadruply bonded dirhenium species, being 2.290(1) Å. With the characterization of **4** and **5**, a series of Re_2^{6+} compounds with guanidinate ligands has been completed using hpp, tbn, and tbo.[67] The

Table 6. Crystallographic structure parameters for rhenium guanidinate compounds.

Compound	**4**	**5**	**6·3CHCl$_3$**	**8**
Chemical formula	$Re_2C_{24}H_{40}Cl_2N_{12}$	$Re_2C_{20}H_{32}Cl_2N_{12}$	$Re_2C_{27}H_{43}Cl_{12}N_{12}$	$Re_2C_{31}H_{48}N_{12}F_9O_9S_3$
Fw	940.0	883.8		1372.4
Space group	*I*-4	*I*4/m	*P*-i	*C*mma
a (Å)	9.663(3)	8.977(3)	10.046(8)	17.58(2)
b (Å)	9.663(3)	8.977(3)	10.935(8)	16.89(2)
c (Å)	15.425(7)	15.360(6)	13.492(10)	17.69(3)
a (°)	90	90	85.47(1)	90
b (°)	90	90	79.66(1)	90
g (°)	90	90	79.02(1)	90
V (Å^3)	1440.4(10)	1237.8(8)	1429.8(19)	5253(12)
Z	2	2	2	4
d_{calcd} (g·cm^{-3})	2.167	2.371	1.965	1.736
μ (mm^{-1})	8.621	10.024	5.249	4.758
T (K)	213	213	213	213
R1[a] (wR2[b])	0.0639 (0.1287)	0.0411 (0.0740)	0.0849 (0.1587)	0.0939 (0.2049)

[a] R1 = [? $w(F_o - F_c)^2$/? wF_o^2]$^{1/2}$.
[b] wR2 = [? [$w(F_o^2 - F_c^2)^2$]/ ? $w(F_o^2)^2$]$^{1/2}$, $w = 1/[¤^2(F_o^2) + (aP)^2 + bP]$, where $P = [\max(F_o^2,0) + 2(F_c^2)]/3$.

Table 7. Important bond distances for rhenium guanidinate compounds.

Compound	**4**	**5**	**6**	**8**
Re-Re (Å)	2.212(2)	2.290(1)	2.260(1)	2.183(3)
Re-N (Å)	2.079 (avg)	2.068(6)	2.053 (avg)	2.04 (avg)
Re-X (axial ligand)	2.641(4) (Cl^-)	2.565(3) (Cl^-)	2.516(2) (Cl^-)	2.430(18) (O_3SCF_3)

change in the Re–Re bond distance traveling along this series is uneven. Exchanging tbn for hpp increases the distance from 2.191(1) Å to 2.212(2) Å, while the analogous compound with the tbo ligand features a Re–Re distance of 2.290(1) Å. The bite angles measured in the crystal structure are 117, 123, and 128° for the hpp, tbn, and tbo ligands, respectively. As was the case with Ru_2^{6+}, equal changes in the ligand bite angle do not correlate with equal changes in the Re–Re distance.[68] While the differences in the bond length in the diruthenium compounds were presumed to be due to a change in the molecular orbital structure, all of the Re_2^{6+} compounds are observed to be diamagnetic, with a proposed $\sigma^2\pi^4\delta^2$ electronic configuration. The context of scale is important to keep in mind, as the Re–Re distance increases by 0.10 Å from hpp to tbo, while the Ru–Ru distance increases by 0.18 Å across the ligand series. This difference is likely due to the quadruple bond present in these dirhenium compounds being more resistant to lengthening than the triple bond (or for tbo, single) present in the analogous diruthenium compounds.

Compound **6** represents one of a small but growing number of Re_2^{7+} complexes to be structurally characterized.[65] Shown in Figure 12, this oxidized species crystallizes in space group *P*i and has a Re–Re distance of 2.260(1) Å. The increase of 0.05 Å is consistent with the removal of a δ electron,[69] giving this paramagnetic compound a formal bond order of 3.5. Further characterization of this cation was performed on **7**, as the only expected difference between the two is the uncoordinated anion in solution.

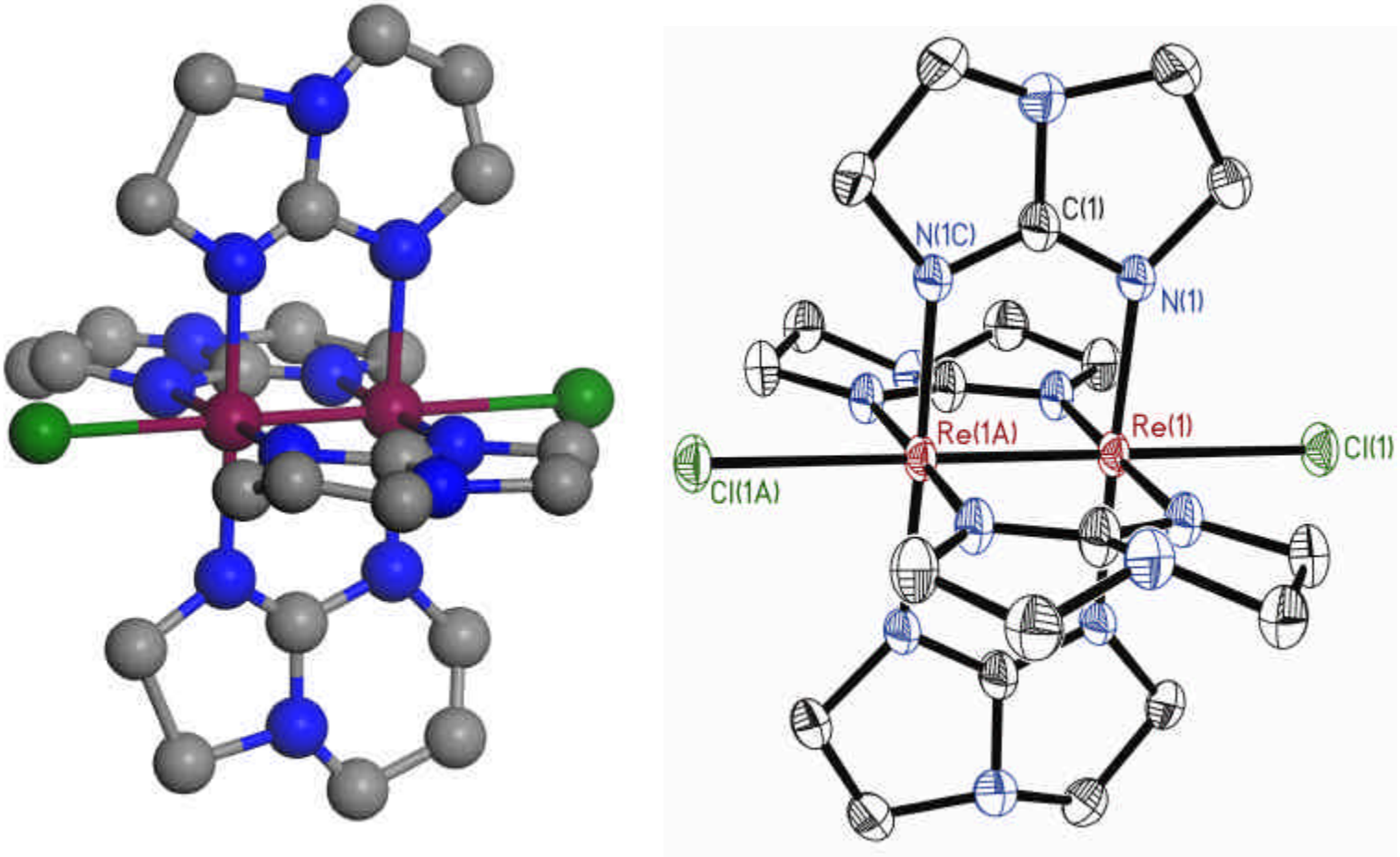

Figure 11. Structural diagrams of **4** and **5**. The thermal ellipsoids for **5** are drawn at the 30% probability level. Hydrogen atoms are omitted for clarity.

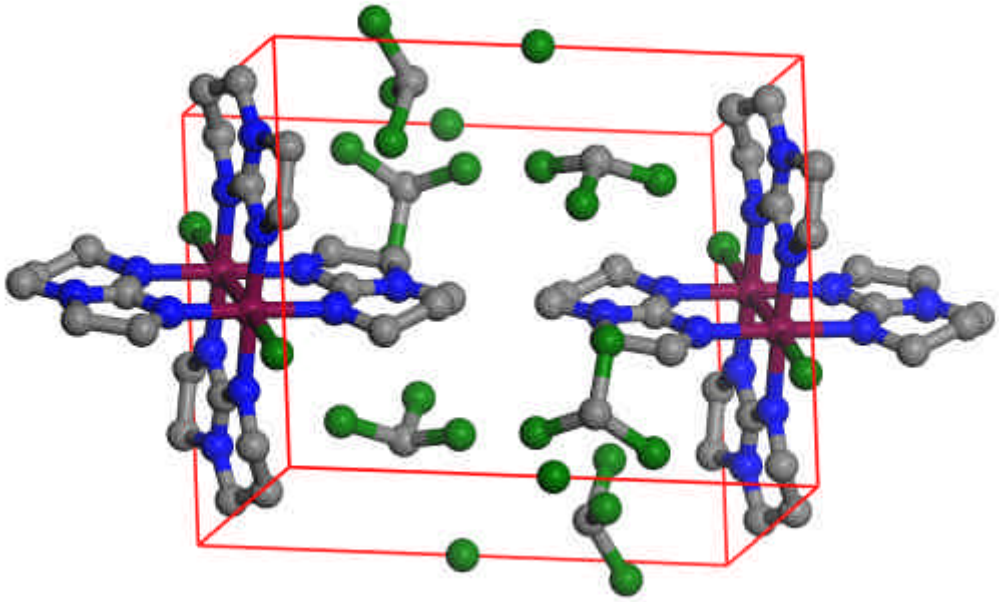

Figure 12. The unit cell diagram of **6**·3$CHCl_3$.

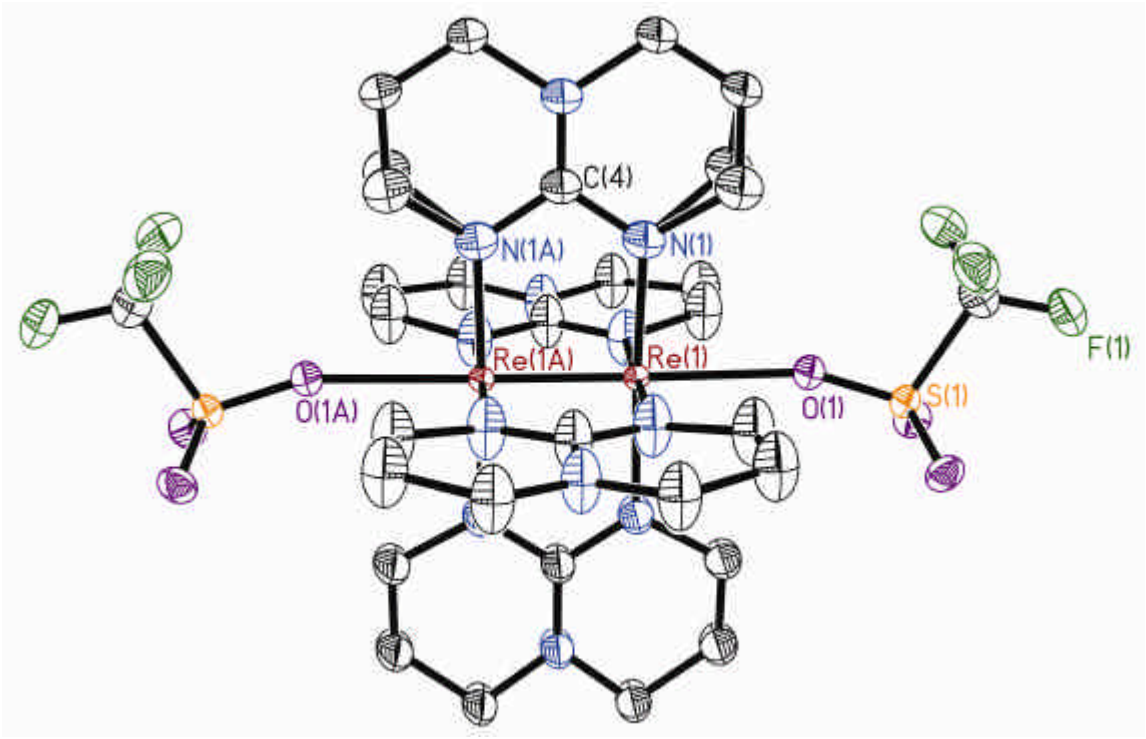

Figure 13. Thermal ellipsoid diagram of **8,** drawn at the 30% probability level. Hydrogen atoms are omitted for clarity.

Compound **8** is also a Re_2^{7+} species, in this case containing three triflate anions as shown in Figure 13. As such, it is more applicable to compare this structure to one previously reported, $[Re_2(hpp)_4](O_3SCF_3)_2$.[21] The presence of two triflate ligands in the axial position of that compound produced a Re–Re distance of 2.1562(7) Å, the shortest yet reported. The oxidized compound **8** has a metal-to-metal bond length of 2.1820(4) Å. While the increased length is slightly lower than the expected range for removal of a δ electron (~0.03-0.05 Å), removal of electrons from other orbitals would yield even larger differences. The predicted electron configuration for **8** is thus $\sigma^2\pi^4\delta^1$. The short Re–Re distances for both compounds are attributed to the decreased electron density donated by the triflate ligands relative to chloride ions.

Electrochemistry. The electrochemical properties of these dirhenium compounds are examined for those compounds that have chlorides in the axial position, with the results shown in Figure 14. In a previous study[67] $Re_2(hpp)_4Cl_2$ was reported to have a CV that contained two reversible waves at +58 and +733 mV, corresponding to the 7+/6+ and 8+/7+ redox events respectively. The CV of **4** is very similar to that of the hpp analogue, containing two reversible waves at +148 and +716 mV. Surprisingly, despite the 7+/6+ couple being ~100 mV higher, the oxidation to the proposed Re_2^{8+} cation is measured to be easier using the tbn ligand rather than hpp. The CV of **5** shows a marked shift to higher potentials with the waves, still reversible, appearing at +423 and +892 mV. Again there is the same unexpected result, as the large shift in the 7+/6+ couple (~300 mV) is paired with a smaller shift (~150 mV) in the 8+/7+ couple. The proposed cause of this behavior lies in the fact that the HOMO for these compounds

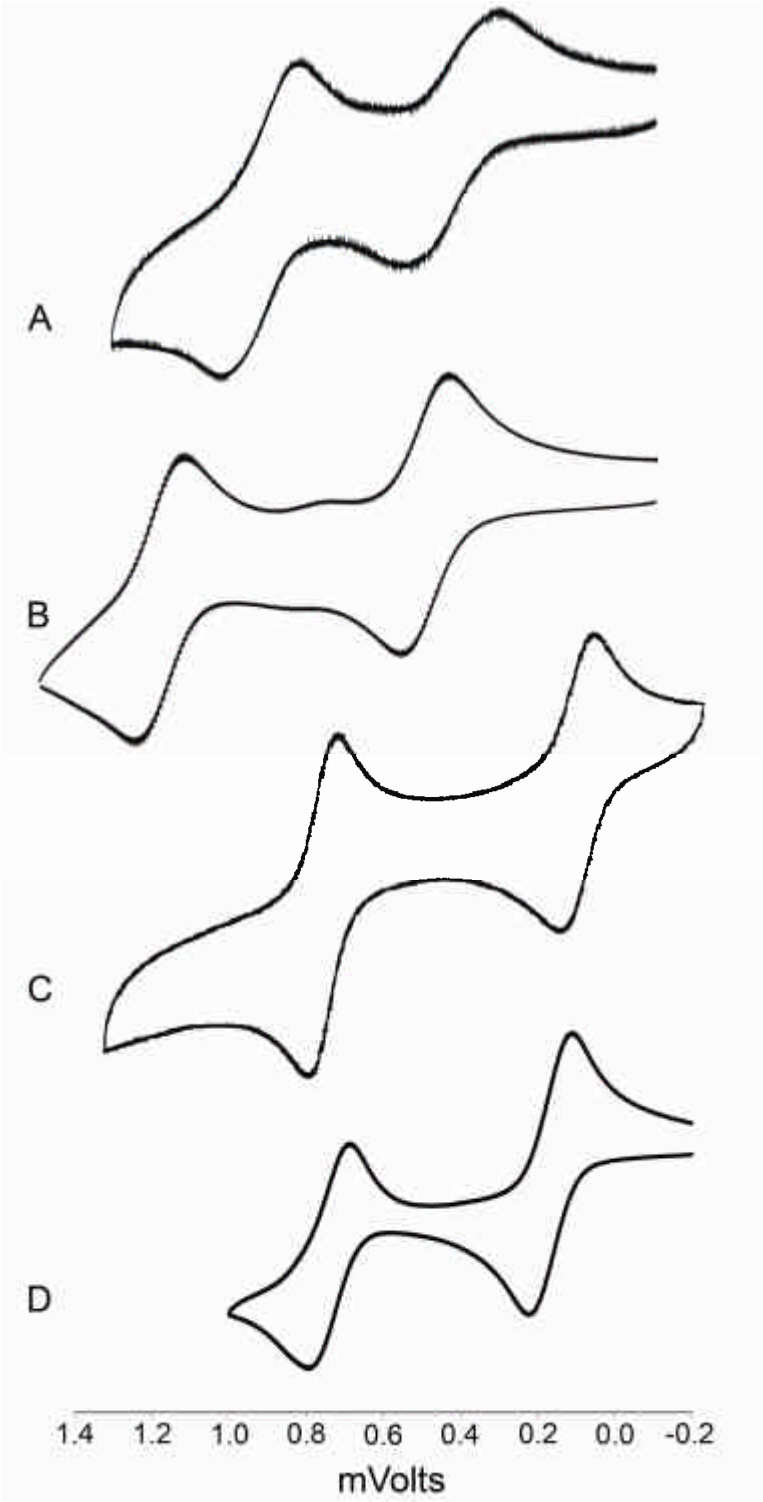

Figure 14. The cyclic voltammograms of several dirhenium guanidinates: a) **8**; b) **5**; c) $Re_2(hpp)_4Cl_2$;[70] and d) **4**. All potentials are vs. Ag/AgCl.

(that is those having eight metal based electrons) has δ symmetry. As has been previously shown, the N p-π orbitals of bicyclic guanidinate ligands strongly interact with δ orbitals, raising them in energy and making it easier to remove electrons.

In the case of **4**, the divergent bite angle of the ligand reduces the overlap between these orbitals, causing the first oxidation process to be at a higher potential. However, as the rhenium atoms move farther apart, the ligand-metal overlap is increased, making the second oxidation step easier than otherwise predicted and decreasing the $\Delta E_{1/2}$. The same reasoning can be used to explain the CV of **5**, where the more divergent tbo ligand shifts the 7+/6+ couple to even higher potential, but the expected increased bond distance upon oxidation improves the overlap between metal atoms and ligands to temper the increase of the 8+/7+ oxidation. While this seems to be an acceptable qualitative explanation, a series of theoretical experiments would need to be performed for confirmation, as well as collecting the structural information for an $[Re_2(tbo)_4Cl_2]^+$ cation. Based on the earlier reported oxidation potentials for $Re_2(hpp)_4(O_3SCF_3)_2$ (+456 and +969 mV), there may be an upper limit to how high the 8+/7+ couple can go before the Re_2^{8+} state becomes inaccessible in this type of system.

Conclusions

The series of $Re_2(LL)_4Cl_2$ compounds where LL = hpp, tbn, or tbo has now been expanded. With compounds **4** and **5**, there are now three examples of this series: $Mo_2(LL)_4$, $Ru_2(LL)_4Cl_2$, and $Re_2(LL)_4Cl_2$. In each case, as the bite angle of the bridging ligand is increased, the M–M distance increases, more so for tbo than for tbn. The bond order present is a determining factor in how greatly the bond length will change. Two

Re_2^{7+} compounds were also characterized structurally, confirming that the ground state configuration is $\sigma^2\pi^4\delta^2$ for the parent Re_2^{6+} species. Future work in this area will include EPR studies on the paramagnetic Re_2^{7+} compounds, as well as theoretical work to model the amount of interaction between the Np-π orbitals of the ligands with the δ orbitals of the rhenium atoms. This work will hopefully lead up to the preparation of a species with an unprecedented Re_2^{8+} core.

CHAPTER V

UNUSUAL MAGNETISM OF AN UNSYMMETRICAL TRINICKEL CHAIN*

Introduction

Ever since the initial discovery by Aduldecha and Hathaway[71] that the anion of 2,2'-dipyridylamine (dpa) can stabilize linear trinickel coordination compounds, a number of related compounds having the general formula $M_3(dpa)_4X_2$ have been prepared with a variety of metal atoms (M = Cr,[72] Co,[73] Cu,[74] Ru,[75] Rh;[76] X may be a variety of axial ligands such as Cl, Br, CN, PF_6 and so on). These trinuclear compounds are members of the family of compounds referred to as *extended metal atom chains* (EMACs).[77] Compounds of this type with several metal atoms, such as those with nine nickel atoms, have also been reported.[78] In our laboratory an important goal has been the elucidation of their fundamental properties. Several compounds having the formula $Ni_3(dpa)_4X_2$, where X represents different axial ligands, have been synthesized and characterized[71,79] as well as analogues having Ni_3^{6+} EMACs with the chain closely cocooned by two interlocking heptadentate dianions.[80] Most of the compounds having Ni_3^{6+} units reported thus far have essentially symmetrical structures (Scheme 4, a). While much effort has been placed in understanding axial ligand exchange processes, less attention has been given to the preparation of less symmetrical species, e. g., those

* Portions of this chapter are reprinted in part from *Eur. J. Inorg. Chem.* **2008** (33), 5257. Cotton, F. A.; Murillo, C. A.; Wang, Q.; Young, M. D. "Unusual Magnetism of an Unsymmetrical Trinkel Chain." Copyright 2008, with permission from Wiley-VCH.

having different ligands on each axial position (Scheme 4, b), or those with an open axial position (Scheme 4, c). The only known unsymmetrical Ni_3^{6+} complex was prepared in very low yield (8%) using the unsymmetrical ligand *N*-phenyl-(2-pyridyl)formamidinate (PhPyF).[81] In $[Ni_3(PhPyF)_4Cl]Cl$ (Scheme 5) the central and one of the outer Ni atoms are essentially square planar but the other outer Ni atom is 5-coordinate. The room temperature magnetic susceptibility showed a magnetic moment of 3.08 μ_B that corresponds to two unpaired electrons, which presumably arise from the terminal 5-coordinate unit.

Scheme 4. A simplified representation of EMACs and the polypyridine ligand not showing the characteristic helical twist.

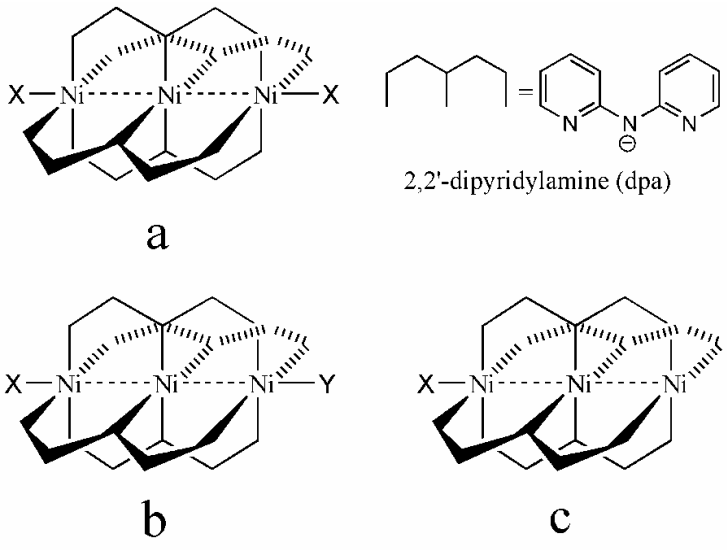

Scheme 5. A portion of the cation $Ni_3(PhPyF)_4Cl^+$ in $[Ni_3(PhPyF)_4Cl]Cl$. There are other two PhPyF ligands perpendicular to the plane, and the central and one of the outer Ni atoms are square planar but the outer Ni atom with the axial chloride group is 5-coordinate. See ref. [81].

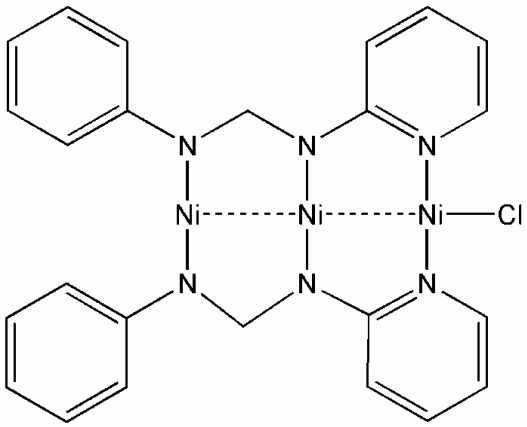

Unsymmetrical species are of interest because axial ligands may influence electronic structures, electrochemistry and magnetic properties of these species[82] and therefore provide a way to tune desirable physical properties. Here is described the preparation and structural characterization of a compound, $[Ni_3(dpa)_4(CH_3CN)](PF_6)_2$ (**1**), which was prepared in good yield and study the effect of a weakly coordinated axial ligand on the electronic structure and magnetic properties of this EMAC.

Experimental

Materials and Methods. All reactions and manipulations were carried out under dry nitrogen using standard Schlenk techniques. Solvents were either distilled over appropriate drying agents in a nitrogen atmosphere or purified using a Glass Contour solvent system. Chemicals were purchased from Aldrich. Anhydrous nickel chloride and silver(I) hexafluorophosphate were dried overnight under vacuum at 70 ºC and 2,2'-dipyridylamide was sublimed prior to use. The symmetrical starting material $[Ni_3(dpa)_4(CH_3CN)_2](PF_6)_2$ was prepared as reported.[79e]

Physical and Characterization Measurements. Elemental analysis was performed by Robertson Microlit Laboratories, Madison, NJ on crystalline samples that had been dried under vacuum. Mass spectrometric data were recorded at the Laboratory for Biological Mass Spectrometry at Texas A&M University. The UV-vis spectrum was measured on a Shimadzu UV-2501PC spectrophotometer in dichloromethane solution. Variable temperature magnetic susceptibility measurements were performed on a Quantum Design SQUID magnetometer MPMS-XL from 2 to 300 K using crushed crystalline samples.

Preparation of $[Ni_3(dpa)_4(CH_3CN)](PF_6)_2 \cdot 2CH_2Cl_2$, $9 \cdot 2CH_2Cl_2$. To a flask containing a crystalline sample of purple $[Ni_3(dpa)_4(CH_3CN)_2](PF_6)_2$ (120 mg, 0.100 mmol) was added 15 mL of dichloromethane. The resulting purple solution was stirred overnight, and the solvent was then removed at ambient temperature under vacuum. The remaining deep purplish red solid was washed with hexanes (2 × 15 mL) and ether (2 × 15 mL), and then dissolved in CH_2Cl_2 (10 mL). A layer of hexanes (30 mL) was added on top of the solution. Deep purplish-red crystals formed within a week. Yield: 92 mg, 68%. Anal. calcd. for $C_{42.5}H_{36}ClF_{12}N_{13}Ni_3P_2$ (**9**·$0.5CH_2Cl_2$): C, 41.50; H, 2.95; N, 14.80%. Found: C, 41.96; H, 2.71; N, 14.86%. Mass spectrum, ESI^+ (m/z): 428.05 for $[Ni_3(dpa)_4]^{2+}$. UV–vis in CH_2Cl_2, $?_{max}$ (nm) (e, $M^{-1}cm^{-1}$): 450 (750), 520 (3000).

X-ray Structural Determination. A suitable crystal was mounted at the end of a quartz fiber with the aid of a small amount of Paratone-N oil and then placed on a

Table 8. Crystallographic data for **9**·2CH_2Cl_2.

	9·2CH_2Cl_2
Empirical formula	$C_{44}H_{39}Cl_4F_{12}N_{13}Ni_3P_2$
M_r	1357.75
Crystal system	triclinic
Space group	*P*i
a [Å]	16.152(5)
b [Å]	19.595(6)
c [Å]	19.984(6)
a [°]	96.656(5)
ß [°]	111.920(5)
? [°]	107.988(5)
V [Å^3]	5386(3)
Z	4
T [K]	213
? [Å]	0.71073
d_{calcd} [g·cm^{-3}]	1.674
F (000)	2736
Crystal size (mm)	0.22 × 0.21 ×0.11
Reflections collected	47772
Independent reflections	19666
Parameters	1382
R_{int}	0.0317
Completeness	98.4%
Goodness-of-fit on F^2	1.016
R1,[a] wR2[b] (I>2s I)	0.0687, 0.1912
R1,[a] wR2[b] (all data)	0.1091, 0.2356

[a] $R1 = S\|\|F_o\|-\|F_c\|\| / S|F_o|$. [b] $wR2 = [S[w(F_o^2-F_c^2)^2]/S[w(F_o^2)^2]]^{1/2}$

goniometer head. X-ray diffraction data for **9**·2CH_2Cl_2 were collected at 213 K on a Bruker SMART 1000 CCD area detector system.[22] Data reduction and integration were performed using the software SAINTPLUS.[23] Absorption corrections were applied using the program SADABS.[24] The structure was solved by direct methods and refined using the SHELXL-97 program.[25] Subsequent cycles of least-squares refinement followed by

difference Fourier syntheses revealed the positions of the remaining non-hydrogen atoms. Hydrogen atoms were added at calculated positions based on a riding model. Non-hydrogen atoms, except some disordered atoms, were refined with anisotropic displacement parameters. Crystallographic data for **9**·2CH_2Cl_2 are given in Table 8.

Results and Discussion

Synthesis and Spectral Characterization. The symmetrical starting material $[Ni_3(dpa)_4(CH_3CN)_2](PF_6)_2$,[79e] synthesized by reacting $Ni_3(dpa)_4Cl_2$[83] with two equivalents of $AgPF_6$ in acetonitrile, was used to generate the unsymmetrical target product, $[Ni_3(dpa)_4(CH_3CN)](PF_6)_2$ (**9**), by simply stirring the symmetrical species in dichloromethane at ambient temperature overnight followed by elimination of the solvent under vacuum, in a process that also removed an axial acetonitrile molecule. During the dissolution process in dichloromethane the color of the solution slowly changed from purple to purplish red. Large block-shaped, purplish red crystals of **9**·2CH_2Cl_2 were obtained after a layer of hexanes was added to a CH_2Cl_2 solution of the crude product.

Compound **9** is air and moisture stable, readily soluble in CH_2Cl_2 and methanol, and its purity was clearly established by a satisfactory elemental analysis. In addition, ESI mass spectrometry shows only one signal at 428.05 *m/z* having the appropriate isotope distribution for the $[Ni_3(dpa)_4]^{2+}$ ion. The electronic spectrum is quite different from those of previously reported trinickel EMACs. The spectrum in dichloromethane solution shows two absorptions, one at 450 nm and another at 520 nm in the visible region but that of $Ni_3(dpa)_4Cl_2$ has only one absorbance at 520 nm. This is consistent

with a change in the electronic structure of the Ni_3^{6+} chain upon removal of a strongly bound axial ligand.

It should be noted that attempts to remove the axial acetonitrile molecule by placing **9** under vacuum for prolonged periods of time at room temperature were unsuccessful. If the processes was repeated by heating the solid to 130 ºC the only isolable products contained $Ni_3(dpa)_4^{2+}$ units with axially coordinated acetamide ligands. Two such compounds were identified, namely $Ni_3(dpa)_4(OC(CH_3)NH)_2$ and a molecule with a chain-like structure, $[Ni_3(dpa)_4(OC(CH_3)NH)]_n$.[84] The acetamide anions presumably form by reaction of acetonitrile with residual hydroxo-containing groups present in the oven-dried glassware. Reactions of acetonitrile with nucleophiles such as water and diphosphines have been well-documented and are catalyzed by metal centers.[85]

Structural Results. The structure, shown in Figure 15, has the characteristic helical twist of the $Ni_3(dpa)_4^{2+}$ core. Compound **9** crystallizes in the triclinic space group *P*i with Z = 4 and two crystallographically independent, but chemically equivalent molecules. The Ni···Ni separations for one of the independent molecules are 2.3396(11) and 2.3548(12) Å, and very similar to those in the other crystallographically independent molecule (2.3450(11) and 2.3651(12) Å) as shown in Table 9. Importantly these Ni···Ni distances are significantly shorter (~0.10 Å) than the corresponding distances of ca. 2.43 Å in $Ni_3(dpa)_4Cl_2$,[83] but only slightly shorter than those in $[Ni_3(dpa)_4(CH_3CN)_2](PF_6)_2$ (2.376(2), 2.371(2) Å).[79e] Even though the Ni···Ni separations in **9** are fairly short, they are still significantly longer than those in the one electron oxidized species

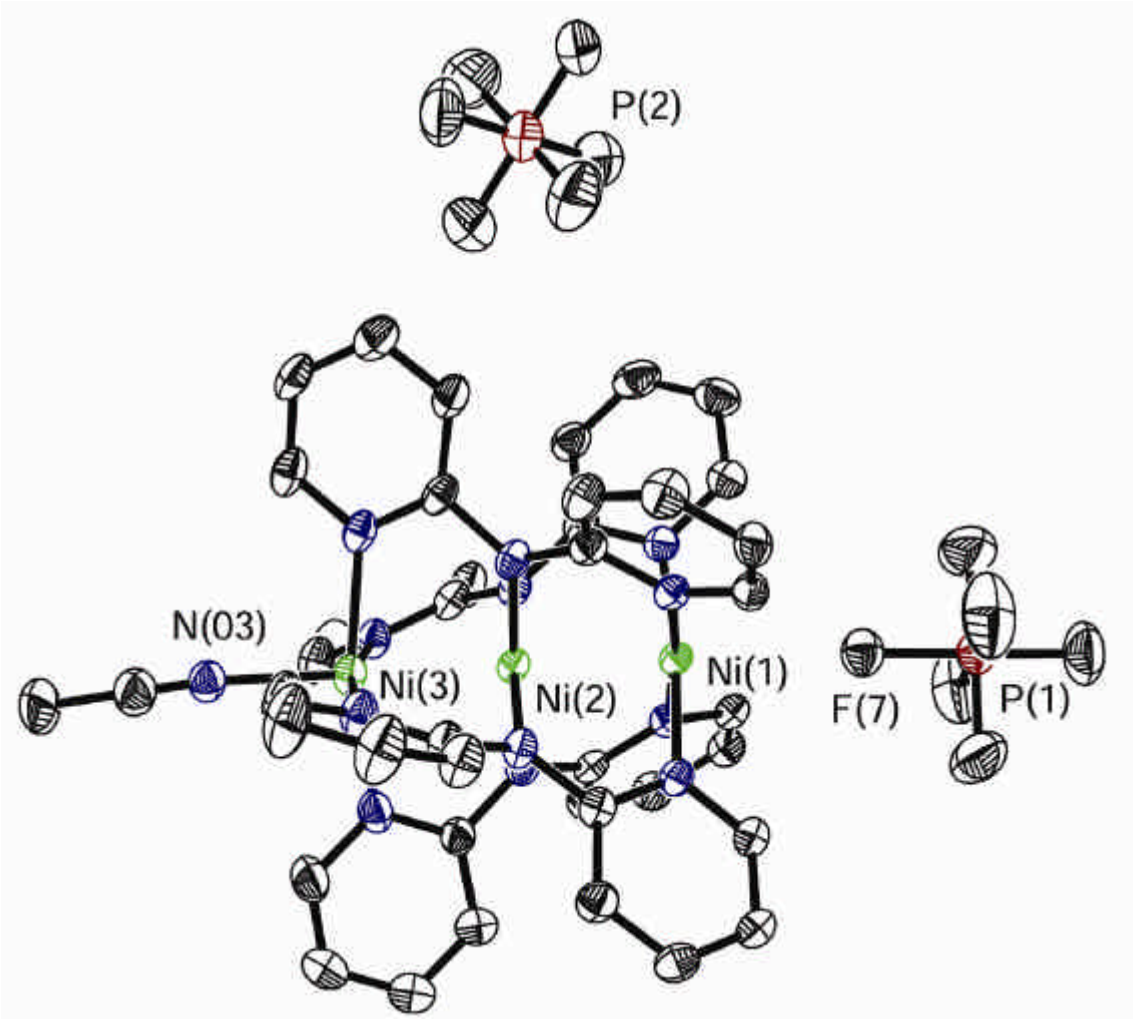

Figure 15. Molecular structure of **9** drawn with ellipsoids at the 40% probability level. All hydrogen atoms have been omitted for clarity. Note that the distance between Ni(1) and F(7) is 2.690 Å while the Ni(3)–N(03) is 2.063(6) Å.

Table 9. Selected bond distances [Å] and angles [°] for the two crystallographically independent molecules in **9**·$2CH_2Cl_2$.

Bond distances			
molecule 1			
Ni(1)···Ni(2)	2.3396(11)	Ni(2)···Ni(3)	2.3548(12)
Ni(1)–N(1)	1.910(5)	Ni(1)–N(4)	1.915(5)
Ni(1)–N(7)	1.912(5)	Ni(1)–N(10)	1.914(5)
Ni(2)–N(2)	1.877(5)	Ni(2)–N(5)	1.878(5)
Ni(2)–N(8)	1.888(5)	Ni(2)–N(11)	1.880(4)
Ni(3)–N(3)	2.108(5)	Ni(3)–N(6)	2.108(5)
Ni(3)–N(9)	2.091(6)	Ni(3)–N(12)	2.089(5)
Ni(3)–N(03)	2.063(6)	Ni(1)···F(1)	2.690
molecule 2			
Ni(4)···Ni(5)	2.3450(11)	Ni(4)···Ni(5)	2.3651(12)
Ni(4)–N(19)	1.910(5)	Ni(4)–N(16)	1.912(5)
Ni(4)–N(13)	1.913(5)	Ni(4)–N(22)	1.926(5)
Ni(5)–N(14)	1.878(5)	Ni(5)–N(23)	1.884(5)
Ni(5)–N(17)	1.896(5)	Ni(5)–N(20)	1.896(5)
Ni(6)–N(15)	2.099(5)	Ni(6)–N(21)	2.095(6)
Ni(6)–N(18)	2.106(5)	Ni(6)–N(24)	2.099(5)
Ni(6)–N(06)	2.061(6)	Ni(4)···F(7)	2.726
Bond angles			
Ni(1)···Ni(2)···Ni(3)	179.33(5)	N(03)–Ni(3)···Ni(2)	177.90(16)
N(1)–Ni(1)–N(7)	174.1(2)	N(10)–Ni(1)–N(4)	173.5(2)
N(5)–Ni(2)–N(11)	176.8(2)	N(2)–Ni(2)–N(8)	176.4(2)
N(9)–Ni(3)–N(3)	166.0(2)	N(12)–Ni(3)–N(6)	166.6(2)
Ni(4)···Ni(5)···Ni(6)	179.19(4)	N(06)–Ni(6)···Ni(5)	178.70(15)

$[Ni_3(dpa)_4(PF_6)_2]PF_6$ (2.2851(6), 2.289(1) Å) that has a 3-center-1-electron bond [86] or in the ethyl-substituted analogue (2.293[4] Å).[87] For comparison, the Ni···Ni separations for some trinickel compounds are given in Table 10. The Ni···Ni···Ni unit in **9** is essentially linear, having an angle of 179.33(5)°.

The atom arrangement for each of the three d^8 Ni atoms in **9** is quite different. For each of the crystallographically independent molecules the central unit is nearly

square planar[88] and the two termini of the molecule being 5-coordinate, square pyramidal. One of the outer Ni atoms has a strongly bound acetonitrile molecule at the apex of the pyramid (Ni(3)–N(03) = 2.063(6) Å and Ni(6)–N(06) = 2.061(6) Å) while the outer has a weakly bound PF_6 anion (Ni(1)···F(1) = 2.690 Å and Ni(4)···F(7) = 2.726 Å). These long distances strongly suggest there is very little interaction between the outer Ni(II) and the fluorine atoms. This is further supported by a comparison of the equatorial Ni–N distances. Those in the central 4-coordinate square unit are, as expected,[77] the shortest (range of 1.877(5) to 1.896(4) Å). For the outer unit bound to the acetonitrile molecule, the corresponding distances are longer by more than 0.2 Å (range of 2.089(5) to 2.108(5) Å). However, the equatorial Ni–N distances for the site with the hexafluorophosphate anion are only slightly longer than those for the central unit (range of 1.910(5) to 1.926(5) Å).

Table 10. Metal···metal separations for some trinickel EMACs.

Compound[a]	Ni···Ni (Å)	ref
$Ni_3(dpa)_4Cl_2 \cdot 2CH_2Cl_2$	2.4386(9), 2.422(1)	83
$Ni_3(dpa)_4(AnCOO)_2$	2.4248(9), 2.2.4220(9)	79h
$Ni_3(dpa)_4(CN)_2 \cdot CH_2Cl_2$	2.4523(3)	79b
$Ni_3(dpa)_4(N_3)_2$	2.4325(7), 2.4356(7)	79f
$[Ni_3(dpa)_4(CH_3CN)_2](PF_6)_2 \cdot 3.14CH_3CN$	2.376(2), 2.371(2)	79e
$[Ni_3(PhPyF)_4Cl]Cl$	2.443(3), 2.454(3)	81
9	2.3396(11), 2.3548(12) 2.3450(11), 2.3651(12)	this work
$[Ni_3(dpa)_4(PF_6)_2]PF_6 \cdot 5CH_2Cl_2$	2.2851(6), 2.289(1)	86
$[Ni_3(depa)_4(PF_6)_2]PF_6 \cdot 3CH_2Cl_2$	2.293[4]	79e

[a] Abbreviations: dpa = the anion of 2,2'-dipyridylamine, AnCOO = the anion of antracene-9-carboxylate, PhPyF = the anion of *N*-phenyl-(2-pyridyl)formamidine, depa = the anion of 4,4'-diethyl-2,2'-dipyridylamine.

Interestingly, the outer square pyramidal units also show important structural differences upon comparison of the distance of the Ni atoms from the idealized square plane formed by the four equatorial nitrogen atoms, shown as *d* in Figure 16. The Ni atom bound to the acetonitrile molecule is pulled 0.239 Å from the plane but that adjacent to the PF_6 anion has a *d* of only 0.097 Å. This difference (vide infra) greatly influences the magnetism. For comparison, the calculated values of *d* for the outer units of other Ni_3^{6+} EMACs are 0.289 and 0.278 Å in $Ni_3(dpa)_4Cl_2$,[17] 0.242 and 0.235 Å in $Ni_3(dpa)_4(CH_3CN)_2$,[79e] 0.238 Å in $Ni_3(depa)_4(CH_3CN)_2$,[79e] 0.279 and 0.289 Å in $Ni_3(dpa)_4(AnCOO)_2$.[79h] For the oxidized species containing Ni_3^{7+} cores, the *d* distances are 0.102 Å for $[Ni_3(dpa)_4](PF_6)_3$,[86] and 0.103 Å for $[Ni_3(depa)_4](PF_6)_3$.[79e] These data show a strong correlation between the value of *d* and how strongly bound is the group in the axial position with those groups such as acetonitrile, chloride and carboxylates having *d* values of 0.23–0.29 Å while those with the weaker donor PF_6 in the range of about 0.1 Å.

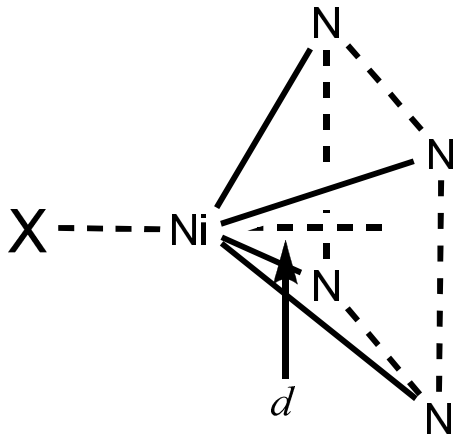

Figure 16. A drawing showing the environment of the outer units in **9**. For a square base of four nitrogen atoms and the out of plane nickel atom, *d* is the distance from the Ni atom to the center of the idealized square base. The axial ligand is represented as X.

It should be noted that how much the outer Ni atoms are pulled from the square plane has important implications in the Ni···Ni separations in these trinickel complexes. Because the central units are typically square planar, the further away from the plane the outer Ni atoms are, the longer the Ni···Ni separation would be expected, and this is clearly seem from the data in Table 10.

In view of these results it is useful to make a comparison of the separation between nickel atoms in the species with Ni_3^{6+} and Ni_3^{7+} cores. As mentioned earlier there are two compounds with an oxidized core, $[Ni_3(dpa)_4](PF_6)_3$[86] and $[Ni_3(depa)_4](PF_6)_3$.[79e] Each has F atoms from PF_6 groups about 2.42–2.45 Å away from the outer Ni atoms. This separation is about 0.25 Å closer than that in **9**, which was assumed to be consistent with the increase in the positive charge of the trinickel unit. Interestingly there is not a significant difference in the distance *d* between the oxidized species and **9**. These results again suggest that the hexaflurophosphate anions have little influence in the electronic environment of the outer units. However, it raises an important issue as to whether the shortening in the Ni···Ni separations in the oxidized species relative to those in the unoxidized species with strongly coordinated groups is due to bond formation as had been suggested,[79,86] or whether this is simply due to the change in coordination of the outer units. If the Ni···Ni separations in **9** are adjusted assuming that the axial Cl atom could be replaced by a second PF_6 these separation would be expected to be very similar to those in the oxidized species.

Although this issue cannot be answered unambiguously by the present data, the increase charge in the oxidized Ni_3^{7+} units would be expected to lead to an increase in

the separation between nickel atoms as is known for the oxidation of $Cu_3(dpa)_4Cl_2$ to $[Cu_3(dpa)_4Cl_2]SbCl_6$.[86] However, upon oxidation of a Ni_3^{6+} to a Ni_3^{7+} core removal of a non-bonding electron would be expected to favor bond formation. It appears the effect of these forces essentially cancels out and the observed distances and those adjusted by the changes in coordination are quite similar. This type of cancellation has been observed frequently in dinuclear paddlewheel compounds.[89] It should also be noted that there is now strong additional evidence for the existence of Ni–Ni bonding in cations of the type $[Ni_2(formamidinate)_4^+]$[90] and in large EMACs such as those containing five nickel atoms.[91]

Magnetism. The variable-temperature magnetic data are shown in Figure 17. The shape of the curves is very different from those resulting from symmetrical Ni_3^{6+} EMACs.[77,82] Studies on a series of symmetrical trinickel compounds have shown that the ?*T* values are less than 2.00 emu K/mol for two independent *S* = 1 centers, which suggests that the spins are partially randomized at high temperature.[77,82] Each of the two terminal Ni atoms contribute two unpaired electrons while the central Ni atom does not supply unpaired electrons (Scheme 6a) because of its d^8 square planar unit that resembles the $Ni(CN)_4^{2-}$ anion.[92] The ?*T* values decrease as the temperature decreases, and ?*T* values are essentially zero below 50 K because of antiferromagnetic coupling. However, in **9** the ?*T* values are about 1.20 emu K/mol at room temperature, and do not significantly decrease as the temperature decreases to ca. 25 K. The magnetic data strongly suggest that the small pull from the square planar plane of the Ni atom in the vicinity of the PF_6 anion does not have important consequences to the magnetism above

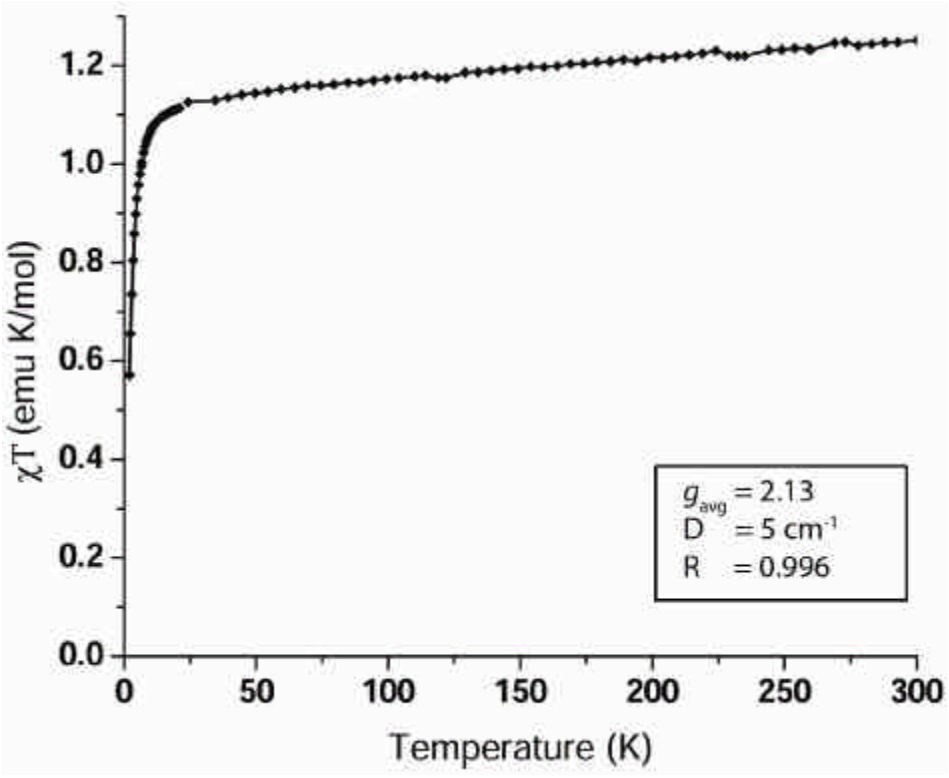

Figure 17. Magnetic susceptibility data for **1** in the range of 2 to 300 K. See text for details on the fitting.

25 K, and this unit can be considered as behaving as a square planar species. Thus **9** is unusual among the family of Ni_3 EMACs in that it has Curie-like magnetism; that is, the magnetic behavior observed arises from an S = 1 state of the pyramidal nickel atom coordinated by the acetonitrile ligand, represented in Scheme 6b. Under this description, the magnetic data was fit using the equation

$$c = \frac{Nb^2g^2}{kT} \cdot \frac{\left(e^{-D/kT} + \left(\frac{2kT}{D} \right) \left(1 - e^{-D/kT} \right) \right)}{\left(1 + 2e^{-D/kT} \right)} \qquad \textbf{(3)}$$

where *D* is the ZFS parameter, *k* is the Boltzmann constant, *N* is Avogadro's number, and ß is the Bohr magneton. The fitting was done for the temperature range of 2 – 20 K to minimize the interference from temperature independent paramagnetism, likely due to a small amount of paramagnetic impurity. Under these conditions, g_{avg} was calculated to be 2.13, while $D = -5\ cm^{-1}$ is responsible for the drop in χT under 25 K.

Scheme 6. The electrons in an EMAC with a) two terminal 5-coordinate units and b) with only one such unit.

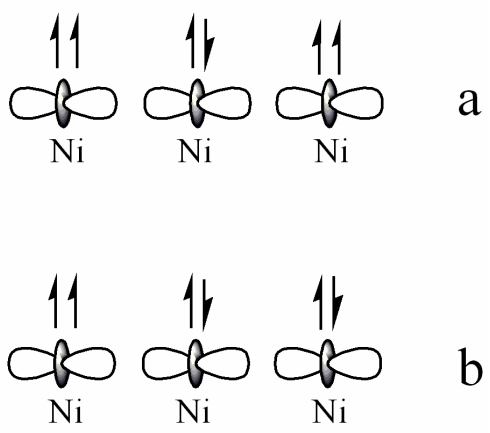

Conclusions

The present study shows that an unsymmetrical Ni_3^{6+} EMAC having only one strongly bound axial ligand can be synthesized in good yield. The electronic spectrum and magnetic properties of this Ni_3^{6+} chain which has a weakly bound axial ligand is greatly changed relative to those having two strongly bound axial ligands. One terminal Ni atom in **9** is paramagnetic with two unpaired electrons due to the square pyramidal coordination, while the other terminal Ni atom and the central Ni atom are diamagnetic

and nearly square planar. This shows that magnetic behavior in this type of EMACS can be tuned by the electron donor ability of the axial ligands.

CHAPTER VI

CONCLUSIONS

Structural Effects of the tbn and tbo Ligands

The three chapters dealing with guanidinate ligands each focused on a separate property. Chapter II focused on changes in the electronic configuration of $[Ru_2]^{6+}$ compounds as the different ligands were used. Chapter III examined the unusual EPR spectra of $[Os_2(hpp)_4Cl_2]^{+}$ and how it related to the crystal structure. Finally, Chapter IV delved into the relationship between the molecular structure and electrochemistry of $[Re_2]^{n+}$ compounds. This information, specifically Chapters II and IV, can now be combined with previous work to better understand some characteristics of bicyclic guanidinate ligands in dimetal compounds.

During the initial investigation of the use of Htbn and Htbo as ligands for dimetal compounds, the Mo_2^{n+} core (n = 4, 5, 6) was used as a common base from which comparisons could be made.[8] The choice was well made, as this system allowed study of up to three stable oxidations states of the dimetal unit for each ligand used. At the conclusion of that report, a prediction was made for the expected metal-to-metal bond lengths in $Ru_2(LL)_4Cl_2$ guanidinate systems. These predictions were based on the bite angle of the ligand as they were measured in a DFT calculation and applied to the experimental Ru-Ru distance measured in $Ru_2(hpp)_4Cl_2$. That table of calculated bond

lengths is reproduced in Table 11, now expanded with the experimentally measured distances.

Table 11. A comparison of predicted vs. actual Ru-Ru bond lengths.

Compound	Predicted Ru-Ru Distance (Å)	Experimental Ru-Ru Distance (Å)
$Ru_2(hpp)_4Cl_2$	---	2.324
$Ru_2(tbn)_4Cl_2$	2.339	2.387
$Ru_2(tbo)_4Cl_2$	2.392	2.501

It is easily seen that these predictions went erroneous quickly, with the predicted Ru-Ru distance in the tbo compound incorrect by over one-tenth of an angstrom. It is likely that the cause of the large discrepancy is due to basing part of the prediction on the Mo_2^{4+} results. This resulted in a Mo_2^{4+} system with a bond order of four being compared to a Ru_2^{6+} system with bond orders of three or one. A more applicable comparison would be to the Re_2^{6+} family of compounds which also have a bond order of four. This comparison is made in Table 12, which also includes the measured N-C-N bite angle of the guanidinate bridging ligands.

Table 12. Metal-to-metal distances for a series of guanidinate compounds.

Compound	M-M Distance (Å)	% Increase over $M_2(hpp)_4Cl_2$	Ligand N-C-N Angle (°)	Bond Order
$Mo_2(hpp)_4$	2.067	---	117	4
$Mo_2(tbn)_4$	2.082	0.73	123	4
$Mo_2(tbo)_4$	2.132	3.15	128	4
$Re_2(hpp)_4Cl_2$	2.191	---	117	4
$Re_2(tbn)_4Cl_2$	2.212	0.96	123	4
$Re_2(tbo)_4Cl_2$	2.290	4.52	128	4
$Ru_2(hpp)_4Cl_2$	2.324	---	112	3
$Ru_2(tbn)_4Cl_2$	2.387	2.71	122	3
$Ru_2(tbo)_4Cl_2$	2.501	7.62	131	1

Expanding on the brief analysis in Chapter IV, a closer look can now be taken at how these three guanidinate ligands affect the metal-metal bond distance. The first comparisons will be between the Mo_2^{4+} and Re_2^{6+} compounds, each with a bond order of four. In both sets of compounds the same pattern is observed, with a small distance increase going to tbn, and a larger increase when using tbo as the bridging ligand. Surprisingly, though the M-M bond distance is ~0.13 Å longer in each dirhenium compound compared to dimolybdenum, the N-C-N angles are equivalent. This does not mean that the ligands are not adjusted by the metal-metal distance, as the diruthenium compounds prove. $Ru_2(hpp)_4Cl_2$ has the longest M-M distance out of the three metal systems, yet it also has the smallest N-C-N angle at 112°. The angle in the tbn compound is nearly equal to the other two metals at 122°, yet the tbo N-C-N angle in $Ru_2(tbo)_4Cl_2$ is the largest of its kind at 131°. In light of this information, it does not appear possible to predict the metal-to-metal bond distance based on the bite angle of the ligand. Instead, only a qualitative inference may be made for an individual series of compounds based on the bond length of one species in that series and the bond order of those compounds. To a first approximation, this leads to the unsurprising conclusion that a series of compounds with a high bond order will be less affected by the divergent ligands, while those with lower bond orders will be more affected.

Effect of Axial Ligation

The work with dirhenium guanidinates and the trinickel EMACs highlight the important contributions given by the axial ligands present. With the rhenium compounds, the use of triflate ions in place of chloride ions caused a significant decrease

in the metal-to-metal bond distance. $Re_2(hpp)_4(O_3SCF_3)_2$ also had an interesting change in its electrochemical potentials to much higher values. Similar values were seen for $Re_2(tbo)_4Cl_2$, which has a Re-Re distance 0.14 Å longer than $Re_2(hpp)_4(O_3SCF_3)_2$. In the trinickel EMAC $[Ni_3(dpa)_4(CH_3CN)](PF_6)_2$, removal of one strongly coordinating ligand (CH_3CN or Cl^-) caused the average metal-metal separation to decrease by 0.10 Å. If this decrease is repeated when the second CH_3CN were removed, then the entire decrease in metal-to-metal distances seen in the oxidized EMAC would be due to the axial ligands. Any decrease caused by the 3c-1e$^-$ bond would be offset by the increase nuclear repulsion between the nickel atoms. It was also shown that the PF_6^- ion that resides in the axial position does not affect that terminal nickel atom significantly enough to cause enough deviation from a square planar environment, resulting in a diamagnetic metal center.

Future Work

The future research of these bicyclic guanidinate ligands lies in an even better understanding of their effects on the structural and electrochemical properties of more dimetal species. The current body of work has two sets of compounds, each with a bond order of four, with a third series that experiences a change in its electronic configuration. The examples that will be needed will have low bond orders (one or two). The two best candidates for this are then platinum and palladium, where their respective $M_2(LL)_4Cl_2$ compounds would contain a net single bond. Inferences as to the effect of these ligands on the electrochemistry of these compounds could be accomplished by looking at both

the oxidative and reductive processes. To obtain a series with a bond order of two, iridium would be the metal of choice.

The tbo ligand offers the possibility of some very interesting effects, as was seen in the case of $Ru_2(tbo)_4Cl_2$. Unfortunately, the chief hindrance to more extensive use of this ligand is its extremely poor solubility, both as a free ligand and in paddlewheel complexes. The Mannich reaction used to prepare HTMhpp and HTEhpp would not be applicable here, as the use of an aldehyde necessitates the formation of a six-membered ring. Instead, a condensation reaction could be used to react an aminoalcohol with an ammonium salt to form the desired triamine. There are several organic catalysts that can accomplish this reaction, but it will have to be seen if the steric bulk of four alkyl groups can be accommodated in such proximity.

Future work can be done with the dirhenium guanidinate compounds by continuing the systematic preparation of compounds that have axial triflate ions rather than chloride ions. In this way differences caused by the various bicyclic guanidinate ligands can be taken into account to see which effect is dominant at a given metal-metal distance. The future study of axial ligands in the trinickel EMACs can be done by accomplishing one of the goals not achieved in the present work: namely, the preparation of Ni_3^{6+} chain using dpa that does not have a strong coordinating ligand in the axial positions. Since the removal of acetonitrile was not successful using heat and vacuum, the new preparation should avoid using acetonitrile altogether. Tetrahydrofuran or a similar

solvent should be able to serve for this purpose. The solvent used during the exchange of chloride to PF_6^- must still be able to dissolve the silver salt, but it should not be as strongly coordinating so that it is difficult to remove. Use of another solvent will also help to avoid the side reaction that forms acetamide.

REFERENCES

(1) Cotton, F. A.; Curtis, N. F.; Harris, C. B.; Johnson, B. F. G.; Lippard, S. J.; Mague, T. J.; Robinson, W. R.; Wood, J. S. *Science* **1964**, *145*, 1305.

(2) a) Cotton, F. A.; Curtis, N. F.; Johnson, B. F. G.; Robinson, W. R. *Inorg. Chem.* **1964**, *4*, 326. b) Cotton, F. A.; Harris, C. B. *Inorg. Chem.* **1964**, *4*, 330. c) Cotton, F. A. *Inorg. Chem.* **1964**, *4*, 334.

(3) Cotton, F. A.; Murillo, C. A.; Walton, R. A., Eds. *Multiple Bonds between Metal Atoms, 3rd Ed.*; Springer Science and Business Media, Inc. New York, **2005**.

(4) Cotton, F. A.; Donahue, J. P.; Murillo, C. A. *J. Am. Chem. Soc*. **2003**, *125*, 5436.

(5) (a) Ward, M. D. *Chem. Soc. Rev.* **1995**, *34*, 121. (b) Astruc, D. *Acc. Chem. Res.* **1997**, *30*, 383. (c) McCleverty, J. A.; Ward, M. D. *Acc. Chem. Res.* **1998**, *31*, 842. (d) Li, Z.; Beatty, A. M.; Fehlner, T. P. *Inorg. Chem.* **2003**, *42*, 5707. (e) Biancardo, M.; Schwab, P. F.; Argazzi, R.; Bignozzi, C. A. *Inorg. Chem.* **2003**, *42*, 3966.

(6) Cotton, F. A.; Matonic, J. H.; Murillo, C. A. *J. Am. Chem. Soc.* **1997**, *119*, 7889.

(7) Cotton, F. A.; Gruhn, N. E.; Gu, J.; Huang, P.; Lichtenberger, D. L.; Murillo, C. A.; Van Dorn, L. O.; Wilkinson, C. C. *Science* **2002**, *298*, 1971.

(8) Wilkinson, C. C. *Dissertation*. **2004,** *Texas A&M University*.

(9) Norman, J. G.; Renzoni, G. E.; Case, D. A. *J. Am. Chem. Soc*. **1979**, *101*, 5256.

(10) Bear, J. L.; Li, Y.; Han, B.; Van Caemelbecke, E.; Kadish, K. M. *Inorg. Chem*. **1997**, *36*, 5449.

(11) Xu, G-L.; Ren, T. *J. Organomet. Chem*. **2002**, *655*, 239.

(12) Xu, G-L.; Jablonski, C. G.; Ren, T. *Inorg. Chim. Acta* **2003**, *343*, 387.

(13) Bear, J. L.; Li, Y.; Han, B.; Kadish, K. M. *Inorg. Chem*. **1996**, *35*, 1395.

(14) Cotton, F. A.; Murillo, C. A.; Reibenspies, J. H.; Villagrán, D.; Wang, X.; Wilkinson, C. C. *Inorg. Chem*. **2004**, *43*, 8373.

(15) See for example: Cotton, F. A.; Herrero, S.; Jiménez-Aparicio, R.; Murillo, C. A.; Urbanos, F. A.; Villagrán, D.; Wang, X. *J. Am. Chem. Soc*. **2007**, *129*, 12666 and references therein.

(16) For an example of large zero-field splitting in a Ru_2^{n+} species see: a) Chen, W.-Z.; Cotton, F. A.; Dalal, N. S.; Murillo, C. A.; Ramsey, C. M.; Ren, T.; Wang, X. *J. Am. Chem. Soc*. **2005**, *127*, 12691. b) Cotton, F. A.; Miskowski, V. M.; Zhong, B. *Inorg. Chem.* **1989**, *111*, 6177.

(17) (a) Cotton, F. A.; Murillo, C. A.; Wang, X.; Wilkinson, C. C. *Inorg. Chem*. **2006**, *45*, 5493. (b) Cotton, F. A.; Durivage, J. C.; Gruhn, N. E.; Lichtenberger, D. L.; Murillo, C. A.; Van Dorn, L. O.; Wilkinson, C. C. *J. Phys. Chem. B* **2006**, *110*, 19793.

(18) Cotton, F. A.; Murillo, C. A.; Wang, X.; Wilkinson, C. C. *Dalton Trans*. **2007**, *35*, 3943.

(19) Cotton, F. A.; Murillo, C. A.; Wang, X.; Wilkinson, C. C. *Dalton Trans*. **2006**, *38*, 4623.

(20) Mitchell, R. W.; Spencer, A.; Wilkinson, G. *J. Chem. Soc., Dalton Trans.* **1973**, 846.

(21) For both $Ru_2(tbn)_4Cl_2$ and $Ru_2(tbo)_4Cl_2$, multiple attempts were made to obtain an elemental analysis including nitrogen. Without exceptions, the expected percentages for carbon and hydrogen compositions were satisfactory but the percentage for nitrogen was slightly low. This is not uncommon for species that produce metal nitrides during combustion.

(22) *SMART for Windows NT*, version 5.618; Bruker Advanced X-ray Solutions, Inc.: Madison, WI, 2001.

(23) *SAINT. Data Reduction Software. Version 6.36A*; Bruker Advanced X-ray Solutions, Inc.: Madison, WI, 2001.

(24) *SADABS. Area Detector Absorption and other Corrections Software, Version 2.05*; Bruker Advanced X-ray Solutions, Inc.: Madison, WI, 2001.

(25) Sheldrick, G. M. *SHELXTL, version 6.12*; Bruker Advanced X-ray Solutions, Inc.: Madison, WI, 2002.

(26) Whenever $Ru_2(OAc)_4Cl$ was reacted overnight with Li(tbo) or Li(tbn), there was no reaction and the only isolable compound was the diruthenium starting material.

(27) For some samples, the values of χT were measured at around 0.1 emu·K·mol^{-1}, due to a small amount of paramagnetic impurity. Unfortunately measurement of the NMR spectrum was precluded by the extreme insolubility of this compound in most common organic solvents.

(28) (a) Hohenberg, P.; Kohn, W. *Phys. Rev.* **1964**, *136*, B864. (b) Parr, R. G.; Yang, W. *Density-Functional Theory of Atoms and Molecules*, Oxford University Press: Oxford, 1989.

(29) (a) Becke, A. D. *Phys. Rev. A* **1988**, *38*, 3098. (b) Becke, A. D. *J. Chem. Phys.* **1993**, *98*, 1372. (c) Becke, A. D. *J. Chem. Phys.* **1993**, *98*, 5648.

(30) Lee, C. T.; Yang, W. T.; Parr, R. G. *Phys. Rev. B* **1998**, *37*, 785.

(31) Frisch, M. J.; Trucks, G. W.; Schlegel, H. B.; Scuseria, G. E.; Robb, M. A.; Cheeseman, J. R.; Montgomery, Jr., J. A.; Vreven, T.; Kudin, K. N.; Burant, J. C.; Millam, J. M.; Iyengar, S. S.; Tomasi, J.; Barone, V.; Mennucci, B.; Cossi, M.; Scalmani, G.; Rega, N.; Petersson, G. A.; Nakatsuji, H.; Hada, M.; Ehara, M.; Toyota, K.; Fukuda, R.; Hasegawa, J.; Ishida, M.; Nakajima, T.; Honda, Y.; Kitao, O.; Nakai, H.; Klene, M.; Li, X.; Knox, J. E.; Hratchian, H. P.; Cross, J. B.; Bakken, V.; Adamo, C.; Jaramillo, J.; Gomperts, R.; Stratmann, R. E.; Yazyev, O.; Austin, A. J.; Cammi, R.; Pomelli, C.; Ochterski, J. W.; Ayala, P. Y.; Morokuma, K.; Voth, G. A.; Salvador, P.; Dannenberg, J. J.; Zakrzewski, V. G.; Dapprich, S.; Daniels, A. D.; Strain, M. C.; Farkas, O.; Malick, D. K.; Rabuck, A. D.; Raghavachari, K.; Foresman, J. B.; Ortiz, J. V.; Cui, Q.; Baboul, A. G.; Clifford, S.; Cioslowski, J.; Stefanov, B. B.; Liu, G.; Liashenko, A.; Piskorz, P.; Komaromi, I.; Martin, R. L.; Fox, D. J.; Keith, T.; Al-Laham, M. A.; Peng, C. Y.; Nanayakkara, A.; Challacombe, M.; Gill, P. M. W.; Johnson, B.; Chen, W.; Wong, M. W.; Gonzalez, C.; Pople, J. A. *Gaussian 03*, Revision C.02; Gaussian, Inc.: Wallingford CT, 2004.

(32) (a) Dunning, T. H.; Hay, P. J. In *Modern Theoretical Chemistry. 3. Methods of Electronic Structure Theory*, Schaefer III, H. F., Ed. Plenum Press: New York, 1977; pp.1-28. (b) Woon, D. E.; Dunning, T. H. *J. Chem. Phys.* **1993**, *98*, 1358.

(33) (a) Dunning, T. H. *J. Chem. Phys.* **1989**, *90*, 1007. (b) Woon, D. E.; Dunning, T. H. *J. Chem. Phys.* **1993**, *98*, 1358. (c) Wilson, A. K.; Woon, D. E.; Peterson, K. A.; Dunning, T. H. *J. Chem. Phys.* **1999**, *110*, 7667.

(34) (a) Wadt, W. R.; Hay, P. J. *J. Chem. Phys.* **1985**, *82*, 284. (b) Hay, P. J.; Wadt, W. R. *J. Chem. Phys.* **1985**, *82*, 299.

(35) Cotton, F. A.; Donahue, J. P.; Gruhn, N. E.; Lichtenberger, D. L.; Murillo, C. A.; Timmons, D. J.; Van Dorn, L. O; Villagrán, D.; Wang, X. *Inorg. Chem.* **2006**, *45*, 201.

(36) (a) Cotton, F. A.; Hillard, E. A.; Murillo, C. A. *J. Am. Chem. Soc*. **2003**, *125*, 2026. (b) Cotton, F. A.; Hillard, E. A.; Murillo, C. A.; Wang, X. *Inorg. Chem*. **2003**, *42*, 6063.

(37) (a) Cotton, F. A.; Daniels, L. M.; Falvello, L. R.; Matonic, J. H.; Murillo, C. A. *Inorg. Chim. Acta* **1997**, *256*, 269. (b) Cotton, F. A.; Feng, X.; Murillo, F. A. *Inorg. Chim. Acta* **1997**, *256*, 303

(38) (a) Cotton, F. A.; Daniels, L. M.; Maloney, D. J.; Matonic, J. H.; Murillo, C. A. *Inorg. Chim. Acta* **1997**, *256*, 283. (b) Cotton, F. A.; Li, Z.; Murillo, C. A.; Poplaukhin, P. V.; Reibenspies, J. H. *J. Cluster Sci*. **2008**, *19*, 89

(39) (a) Cotton, F. A.; Durivage, J. C.; Gruhn, N. E.; Lichtenberger, D. L.; Murillo, C. A.; Van Dorn, L. O.; Wilkinson, C. C. *J. Chem. Phys. B* **2006**, *110*, 19793. (b) Cotton, F. A.; Murillo, C. A.; Wang X.; Wilkinson, C. C. *Dalton Trans*. **2007**, 3943.

(40) Cotton, F. A.; Huang, P.; Murillo, C. A.; Wang, X. *Inorg. Chem. Commun*. **2003**, *6*, 121.

(41) Cotton, F. A.; Daniels, L. M.; Murillo, C. A.; Timmons, D. J.; Wilkinson, C. C. *J. Am. Chem. Soc.* **2002**, *124*, 9249.

(42) Cotton, F. A.; Gruhn, N. E.; Gu, J.; Huang, P.; Lichtenberger, D. L.; Murillo, C. A.; Van Dorn, L. O.; Wilkinson, C. C. *Science* **2002**, *298*, 1971.

(43) Bochmann, M.; Cotton, F. A.; Murillo, C. A.; Wilkinson, G. *Advanced Inorganic Chemistry*, 6th Ed. John Wiley & Sons, Inc.: New York, 1999.

(44) Cotton, F. A.; Donahue, J. P.; Gruhn, N. E.; Lichtenberger, D. L.; Murillo, C. A.; Timmons, D. J.; Van Dorn, L. O.; Villagrán, D.; Wang, X. *Inorg. Chem.* **2006**, *45*, 201.

(45) See for example: (a) Foley, S. R.; Yap, G. P. A.; Richeson, D. S. *Polyhedron*, **2002**, *21*, 619. (b) Soria, D. B.; Grundy, J.; Coles, M. P.; Hitchcock, P. B. *J. Organometal. Chem*. **2005**, *690*, 2315. (c) Coles, M. P.; Hitchcock, P. B. *Organometallics* **2003**, *22*, 5201. (d) Coles, M. P.; Hitchcock, P. B. *Dalton Trans*. **2001**, 1169. (e) Coles, M. P.; Hitchcock, P. B. *Inorg. Chim. Acta* **2004**, *357*, 4330. (f) Oakley, S. H.; Coles, M. P.; Hitchcock, P, B. *Inorg. Chem*. **2004**, *43*, 7564. (g) Coles, M. P.; Hitchcock, P. B, *Eur. J. Inorg. Chem*. **2004**, 2662. (h) Irwin, M. D.; Abdou, H. E.; Mohamed, A. A.; Fackler, J. P., Jr. *Chem. Commun*. **2003**, 2882. (i) Feil, F.; Harder, S. *Eur. J. Inorg. Chem*. **2005**, 4438. (j) Wilder, C. B.; Reitfort, L. L.; Abboud, K. A.; McElwee-White, L. *Inorg. Chem*. **2006**, *45*, 263. (k) Rische, D.; Baunemann, A.; Winter, M.; Fischer, R. A.. *Inorg. Chem*. **2006**, *45*, 269.

(46) F. A. Cotton, C. A. Murillo, X. Wang and C. C. Wilkinson, *Inorg. Chim. Acta* **2003**, *351*, 191.

(47) F. A. Cotton, N. S. Dalal, P. Huang, C. A. Murillo, A. C. Stowe and X. Wang, *Inorg. Chem.* **2003**, *42*, 670.

(48) Drago, R. S. *Physical Methods forChemists*, 2nd Ed.; Surfside Scientific Publishers: Gainsville, Fl., 1992.

(49) *SMART for Windows NT*, version 5.618; Bruker Advanced X-ray Solutions, Inc.: Madison, WI, 2001.

(50) *SAINT. Data Reduction Software. Version 6.36A*; Bruker Advanced X-ray Solutions, Inc.: Madison, WI, 2001.

(51) *SADABS. Area Detector Absorption and other Corrections Software, Version 2.05*; Bruker Advanced X-ray Solutions, Inc.: Madison, WI, 2001.

(52) Sheldrick, G. M. *SHELXTL, version 6.12*; Bruker Advanced X-ray Solutions, Inc.: Madison, WI, 2002.

(53) Clérac, R.; Cotton, F. A.; Daniels, L. M.; Donahue, J. P.; Murillo, C. A.; Timmons, D. J. *Inorg. Chem*. **2000**, *39*, 2581.

(54) See for example: Borrás-Almenar, J. J.; Coronado, E.; Gatteschi, D.; Gómez-Garcia, C. J; Zanchini, C. *J. Phys. Chem*. 1993, 97, 4206.

(55) For example, see: (a) Angaridis, P. In *Multiple Bonds between Metal Atoms*, Cotton, F. A.; Murillo, C. A.; Walton, R. A. Eds. Springer Science and Business Media, Inc., New York, 2005. Ch. 9. (b) Barral, M. C.; Herrero, S.; Jiménez-Aparicio, R.; Torres, M. R.; Urbanos, F. A. *Inorg. Chem. Commun*. **2004**, *7*, 42. (c) Ren, T. *Coord. Chem. Rev*. **1998**, *175*, 43. (d) Telser, J.; Drago, *Inorg. Chem*. **1984**, *23*, 3114. (d) Miskowiski, V. M.; Hopkins, M. D.; Winkler, J. R.; Gray, H. R. In *Inorganic Electronic Structure and Spectroscopy*, Solomon, E. I.; Lever, A. B. P. Eds. vol. 2**,** John Wiley & Sons, 1999, Chapter 6. (e) Liu, W.; Nfor, E. N.; Li, Y.-Z.; Zuo, J.-L.; You, X.-Z. *Inorg. Chem. Commun*. **2006**, *9*, 923. (f) Vos, T. E.; Liao, Y. Shum, W. W.; Her, J.-H.; Stephens, P. W.; Reiff, W. M.; Miller, J. S. *J. Am. Chem. Soc*. **2004**, *126*, 11630. (g) Angaridis, P.; Cotton, F. A.; Murillo, C. A. Villagrán, D.; Wang, X. *J. Am. Chem. Soc*. **2005**, *127*, 5008.

(56) See for example: (a) Cotton, F.A.; Donahue, J. P.; Murillo, C. A.; Huang, P.; Villagrán, D. *Z. Anorg. Allg. Chem*., **2005**, *631*, 2606. (b) Cotton, F. A.; Hillard, E. A.; Murillo, C. A. *Inorg. Chem*. **2002**, *41*, 1639. (c) Cotton, F. A.; Dalal, N. S.; Liu, C. Y.; Murillo, C. A.; North, J. M.; Wang, X. *J. Am. Chem. Soc*. **2003**, *125*, 12945.

(57) Walton, R. A. In *Multiple Bonds between Metal Atoms*, Cotton, F. A.; Murillo, C. A.; Walton, R. A. Eds. Springer Science and Business Media, Inc., New York, **2005**. Ch. 6.

(58) Bratton, W. K.; Cotton, F. A. *Inorg. Chem.* **1969**, *8*, 1035.

(59) Cotton, F. A.; Frenz, B. A.; Shive, L. W. *Inorg. Chem.* **1975**, *14*, 649.

(60) Koz'min, P. A.; Surazhskaya, M. D.; Larina, T. B.; Kotel'nikova, A. S.; Misailova, T. V. *Dokl. Phys. Chem.* **1985**, *280*, 114.

(61) Cotton, F. A.; Gage, L. D. *Inorg. Chem.* **1979**, *18*, 1716.

(62) a) Bennett, M. J.; Cotton, F. A.; Walton, R. A. *J. Am. Chem. Soc.* **1966**, *88*, 3866. b) Bennett, M. J.; Cotton, F. A.; Walton, R. A. *Proc. Roy. Soc.* **1968**, *A303*, 175.

(63) See for example: a) Cotton, F. A.; Hillard, E. A.; Murillo, C. A. *J. Am. Chem. Soc.* **2003**, *125*, 2026. b) Cotton, F. A.; Hillard, E. A.; Murillo, C. A.; Wang, X. *Inorg. Chem.* **2003**, *42*, 6063. c) Cotton, F. A.; Dalal, N. S.; Huang, P.; Murillo, C. A.; Stowe, A. C.; Wang, X. *Inorg. Chem.* **2003,** *42*, 670.

(64) Cotton, F. A.; Murillo, C. A.; Wang, X.; Wilkinson, C. C. *Inorg. Chem.* **2006,** *45*, 5493.

(65) Cotton, F. A.; Dalal, N. S.; Huang, P.; Ibragimov, S. A.; Murillo, C. A.; Piccoli, P. M. B.; Ramsey, C. M.; Schultz, A. J.; Wang, X.; Zhao, Q. *Inorg. Chem.* **2007**, *46*, 1718.

(66) Cotton, F. A.; Donahue, J. P.; Lichtenberger, D. L.; Murillo, C. A.; Villagran, D. *J. Am. Chem. Soc.* **2005**, *127*, 10808.

(67) Cotton, F. A.; Gu, J.; Murillo, C. A.; Timmons, D. J. *J. Chem. Soc., Dalton Trans.* **1999**, 3741.

(68) See Discussion in Chapter II

(69) See for example: (a) Cotton, F.A.; Donahue, J. P.; Murillo, C. A.; Huang, P.; Villagrán, D. *Z. Anorg. Allg. Chem*., **2005**, *631*, 2606. (b) Cotton, F. A.; Hillard, E. A.; Murillo, C. A. *Inorg. Chem*. **2002**, *41*, 1639. (c) Cotton, F. A.; Dalal, N. S.; Liu, C. Y.; Murillo, C. A.; North, J. M.; Wang, X. *J. Am. Chem. Soc*. **2003**, *125*, 12945.

(70) Berry, J. F.; Cotton, F. A.; Huang, P.; Murillo, C. A. *J. Chem. Soc., Dalton Trans.* **2003**, 1218.

(71) Aduldecha, S.; Hathaway, B. *J. Chem. Soc., Dalton Trans*. **1991**, 993.

(72) a) Cotton, F. A.; Daniels, L. M.; Murillo, C. A.; Pascual, I. *J. Am. Chem. Soc*. **1997**, *119*, 10223; b) Chen, Y.-H.; Lee, C.-C.; Wang, C.-C.; Lee, G.-H.; Lai, S.-Y.; Li, F.-Y.; Mou, C.-Y.; Peng, S.-M. *Chem. Commun*. **1999**, 1667; c) Clérac, R.; Cotton, F. A.; Daniels, L. M.; Dunbar, K. R.; Murillo, C. A.; Pascual, I. *Inorg. Chem.* **2000**, *39*, 748; d) Berry, J. F.; Cotton, F. A.; Lu, T.; Murillo, C. A.; Roberts, B. K.; Wang, X. *J. Am. Chem. Soc*. **2004**, *126*, 7082; e) Ismayilov, R. H.; Wang, W.-Z.; Wang, R.-R.; Yeh, C.-Y.; Lee, G.-H.; Peng, S.-M. *Chem. Commun*. **2007**, 1121.

(73) a) Yang, E.-C.; Cheng, M.-C.; Tsai, M.-S.; Peng, S.-M. *J. Chem. Soc., Chem. Commun*. **1994**, 2377; b) Cotton, F. A.; Murillo, C. A.; Wang, X. *J. Chem. Soc., Dalton Trans*. **1999**, 3327; c) Clérac, R.; Cotton, F. A.; Daniels, L. M.; Dunbar, K. R.; Kirschbaum, K.; Murillo, C. A.; Pinkerton, A. A.; Schultz, A. J.; Wang, X. *J. Am. Chem. Soc*. **2000**, *122*, 6226; d) Chien, C.-H.; Chang, J.-C.; Yeh, C.-Y.; Lee, G.-H.; Fang, J.-M.; Peng, S.-M. *Dalton Trans*. **2006**, 2106.

(74) a) Wu, L.-P.; Field, P.; Morrissey, T.; Murphy, C.; Nagle, P.; Hathaway, B.; Simmons, C.; Thornton, P. *J. Chem. Soc., Dalton Trans*. **1990**, 3853; b) Pyrka, G. J.; El-Mekki, M.; Pinkerton, A. A. *J. Chem. Soc., Chem. Commun*. **1991**, 84; c) Berry, J. F.; Cotton, F. A.; Lei, P.; Murillo, C. A. *Inorg. Chem*. **2003**, *42*, 377.

(75) a) Kuo, C.-K.; Liu, P.-C.; Yeh, C.-Y.; Chou, C.-H.; Tsao, T.-B.; Lee, G.-H.; Peng, S.-M. *Chem. Eur. J.* **2007**, 13, 1442; b) Kuo, C.-K.; Chang, J.-C.; Yeh, C.-Y.; Lee, G.-H.; Wang, C.-C.; Peng, S.-M. *Dalton Trans.* **2005**, 3696.

(76) Sheu, J.-T.; Lin, C.-C.; Chao, I.; Wang, C.-C.; Peng, S.-M. *Chem. Commun*. **1996**, 315.

(77) Berry, J. F. in *Multiple Bonds between Metal Atoms*, 3rd ed. Cotton, F. A.; Murillo, C. A.; Walton, R. A., *Eds.* Springer Science and Business Media, Inc., New York, **2005**, p. 669.

(78) Peng, S.-M.; Wang, C.-C.; Jang, Y.-L.; Chen, Y.-H.; Li, F.-Y.; Mou, C.-Y.; Leung, M.-K. *J. Magn. Magn. Mater*. **2000**, *209*, 80.

(79) a) Berry, J. F.; Cotton, F. A.; Daniels, L. M.; Murillo, C. A. *J. Am. Chem. Soc*. **2002**, *124*, 3212; b) Berry, J. F.; Cotton, F. A.; Murillo, C. A. *Dalton Trans.* **2003**, 3015; c) Berry, J. F.; Cotton, F. A.; Murillo, C. A.; Roberts, B. K. *Inorg. Chem.* **2004**, *43*, 2277; d) Berry, J. F.; Cotton, F. A.; Murillo, C. A.; *Organometallics* **2004**, *23*, 2503; e) Berry, J. F.; Cotton, F. A.; Lu, T.; Murillo, C. A.; Wang, X. *Inorg. Chem.* **2003**, *42*, 3595; f) Peng, C.-H.; Wang, C.-C.; Lee, H.-C.; Lo, W.-C.; Lee, G.-H.; Peng, S.-M. *J. Chin. Chem. Soc. (Taipei)*, **2001**, *48*, 987; g) Cotton, F. A.; Murillo, C. A.; Wang, Q. *Inorg. Chem. Commun*. **2007**, *10*, 1088; h) Cotton, F. A.; Chao, H.; Li, Z.; Murillo, C. A.; Wang, Q. *J. Organometal. Chem*. **2008**, *693*, 1412.

(80) Cotton, F. A.; Chao, H.; Murillo, C. A.; Wang, Q. *Dalton Trans*. **2006**, 5416.

(81) Cotton, F. A.; Lei, P.; Murillo, C. A. *Inorg. Chim. Acta* **2003**, *351*, 183.

(82) Berry, J. F.; Cotton, F. A.; Murillo, C. A. *Dalton Trans.* **2003**, 3015-3021.

(83) Clérac, R.; Cotton, F. A.; Dunbar, K. R.; Murillo, C. A.; Pascual, I.; Wang, X. *Inorg. Chem*. **1999**, *38*, 2655.

(84) Crystallographic data for $Ni_3(dpa)_4(OC(CH_3)NH)_2$: Tetragonal space group *P*4/m, $a = b = 11.913(1)$, $c = 16.769(2)$ Å, $V = 2379.7(8)$ Å^3. For $[Ni_3(dpa)_4(OC(CH_3)NH)]_n$: Triclinic space group *P*i, $a = 14.370(3)$, $b = 16.755(4)$, $c = 23.098(5)$ Å, a = 97.092(4), ß = 102.085(4), ? = 95.603(4)º, $V = 5353(4)$ Å^3.

(85) a) Cotton, F. A.; Daniels, L. M.; Murillo, C. A.; Wang, X. *Polyhedron* **1998**, *17*, 2781; b) Concolino, T. E.; Eglin, J. L.; Staples, R. J. *Polyhedron* **1999**, *18*, 915.

(86) Berry, J. F.; Cotton, F. A.; Daniels, L. M.; Murillo, C. A.; Wang, X. *Inorg. Chem*. **2003**, *42*, 2418.

(87) Berry, J. F.; Cotton, F. A.; Lu, T.; Murillo, C. A.; Wang, X. *Inorg. Chem*. **2003**, *42*, 3595.

(88) Unlike the great majority of trinickel compounds in which the central nickel atom is in an essentially square planar configuration, in **1** this nickel atom is about 0.062 Å from the plane of the four nitrogen atoms which creates a small structural asymmetry.

(89) See for example: a) Cotton, F. A.; Dunbar, K. R.; Falvello, L. R.; Tomás, M.; Walton, R. A. *J. Am. Chem. Soc*. **1983**, *105*, 4950; b) Berry, J. F.; Bill, E.; Bothe, E.; Cotton, F. A.; Dalal, N. S.; Ibragimov, S. A.; Kaur, N.; Liu, C. Y.; Murillo, C. A.; Nellutla, S.; North, J. M.; Villagrán, D. *J. Am. Chem. Soc*. **2007**, *129*, 1393.

(90) Berry, J. F.; Bothe, E.; Cotton, F. A.; Ibragimov, S. A.; Murillo, C. A.; Villagrán, D.; Wang, X. *Inorg. Chem*. **2006**, *45*, 4396.

(91) Berry, J. F.; Cotton, F. A.; Lei, P.; Lu, T.; Murillo, C. A. *Inorg. Chem*. **2003**, *42*, 3534.

(92) Cotton, F. A.; Wilkinson, G.; Murillo, C. A.; Bochmann, M. *Advanced Inorganic Chemistry*, 6th ed. John Wiley & Sons, Inc., New York, **1999**.

VITA

Mark David Young received his Bachelor of Arts degree in Chemistry from McDaniel College (formerly Western Maryland College) in May 2004. After graduating Magna cum Laude in the American Chemistry Society certified program, he enrolled at Texas A&M University in the fall of that year, where he began his studies in the research group of Dr. F. A. Cotton. He received his Ph.D. in Chemistry in May 2009.

Mr. Young may be reached at his work address:

Department of Chemistry
Texas A&M University
PO BOX 30012
College Station, TX 77842-3012

or e-mailed at: myoung@mail.chem.tamu.edu